

Sonic Hedgehog Is a Remotely Produced Cue that Controls Axon Guidance Trans-axonally at a Midline Choice Point

Highlights

- Shh protein is produced by RGCs in the retina and transported to the optic chiasm
- Shh is secreted by contralateral RGCs at the chiasm to repel ipsilateral RGCs
- The repulsive effect of Shh requires the receptor Boc and signaling mediator Smo
- Remotely produced cues and axon-axon interactions are important in chiasm guidance

Authors

Jimmy Peng, Pierre J. Fabre,
Tiphaine Dolique, Shannon M. Swikert,
Laëtitia Kermasson,
Tomomi Shimogori, Frédéric Charron

Correspondence

frederic.charron@ircm.qc.ca

In Brief

Although axon guidance cues are typically produced locally at the choice point, Peng et al. show that Shh is transported by RGCs from the retina to the optic chiasm to repel ipsilateral RGC axons trans-axonally.



Sonic Hedgehog Is a Remotely Produced Cue that Controls Axon Guidance Trans-axonally at a Midline Choice Point

Jimmy Peng,^{1,2} Pierre J. Fabre,^{1,6} Tiphaine Dolique,¹ Shannon M. Swikert,^{1,3} Laëtitia Kermasson,¹ Tomomi Shimogori,⁴ and Frédéric Charron^{1,2,3,5,7,*}

¹Montréal Clinical Research Institute (IRCM), 110 Pine West Ave., Montréal, QC H2W 1R7, Canada

²Department of Biology

³Integrated Program in Neuroscience

McGill University, Montréal, QC H3A 2B2, Canada

⁴RIKEN Brain Science Institute, Wako, Saitama 351-0198, Japan

⁵Department of Medicine, University of Montréal, Montréal, QC H3T 1J4, Canada

⁶Present address: Department of Basic Neurosciences, University of Geneva, 1205 Geneva, Switzerland

⁷Lead Contact

*Correspondence: frederic.charron@ircm.qc.ca

<https://doi.org/10.1016/j.neuron.2017.12.028>

SUMMARY

At the optic chiasm choice point, ipsilateral retinal ganglion cells (RGCs) are repelled away from the midline by guidance cues, including Ephrin-B2 and Sonic Hedgehog (Shh). Although guidance cues are normally produced by cells residing at the choice point, the mRNA for Shh is not found at the optic chiasm. Here we show that Shh protein is instead produced by contralateral RGCs at the retina, transported anterogradely along the axon, and accumulates at the optic chiasm to repel ipsilateral RGCs. *In vitro*, contralateral RGC axons, which secrete Shh, repel ipsilateral RGCs in a Boc- and Smo-dependent manner. Finally, knockdown of Shh in the contralateral retina causes a decrease in the proportion of ipsilateral RGCs in a non-cell-autonomous manner. These findings reveal a role for axon-axon interactions in ipsilateral RGC guidance, and they establish that remotely produced cues can act at axon guidance midline choice points.

INTRODUCTION

After being received by the retina, visual information is relayed to the brain. In higher vertebrates, visual information exits each eye via retinal ganglion cell (RGC) neurons, whose axons extend toward the midline and meet at an X-shaped commissure at the midline called the optic chiasm before reaching the brain. In animals with frontally positioned eyes, RGC axons from each eye must project to either the contralateral or ipsilateral sides of the brain to preserve the topography from the overlapping visual fields and enable binocular vision (Jeffery, 2001). Thus, the optic chiasm represents a choice point during development, as each RGC axon needs to make a binary decision to either cross or turn away from the chiasm midline.

Studies of axon behavior at midline choice points throughout the nervous system have found that locally produced guidance cues play a major role in directing axon responses (Tessier-Lavigne and Goodman, 1996). When axons reach a choice point, the cues present there bind to the corresponding receptor(s) on the growth cones, creating either an attractive or repulsive response. Attractive responses facilitate crossing the midline and thus promote contralateral projections, while repulsive responses cause the axon to turn away from the midline and remain ipsilateral (Dickson, 2002; Evans and Bashaw, 2010; Flanagan and Van Vactor, 1998; Petros et al., 2008).

In vitro and *in vivo* experiments in mice have so far identified two guidance cues that repel ipsilateral RGC axons at the chiasm: Ephrin-B2 and Sonic Hedgehog (Shh) (Fabre et al., 2010; Williams et al., 2003). The respective receptors of each repulsive cue, EphB1 and Boc, are expressed only by ipsilateral RGCs, and application of either cue to an RGC explant culture results in selectively reduced growth or growth cone collapse in the ipsilateral RGC population. *In vivo*, knockout mice of either the EphB1 or Boc receptor have a reduced proportion of the ipsilateral RGC population.

Despite these similarities between these two repulsive guidance pathways, the expression pattern of Shh itself is poorly characterized compared to Ephrin-B2, which poses a challenge for our understanding of Shh-mediated ipsilateral RGC axon guidance. Ephrin-B2 is well established as being produced by radial glial cells that reside just dorsal to the optic chiasm and extend processes downward into the optic chiasm, which is later traversed by RGC axons during development (Marcus and Mason, 1995; Williams et al., 2003). In contrast, multiple studies have established that Shh mRNA is conspicuously absent at the level of the optic chiasm itself (Macdonald et al., 1997; Torres et al., 1996; Trousse et al., 2001), despite its presence at the midline in other parts of the nervous system.

The presence of Ephrin-B2 mRNA but absence of Shh mRNA at the optic chiasm suggest fundamental mechanistic differences between the two pathways, and uncovering the source of Shh protein at the chiasm would help to clarify these



differences. Intriguingly, multiple studies have found that RGCs themselves express Shh, with *Shh* mRNA detected at the ganglion cell layer in the retina (Jensen and Wallace, 1997; Wallace and Raff, 1999; Wang et al., 2005; Zhang and Yang, 2001). Some of these studies also note that Shh protein is transported anterogradely along RGC axons and has a proliferative effect on astrocytes surrounding the optic nerve (Dakubo et al., 2008; Wallace and Raff, 1999), while radiolabeling experiments have detected retina-derived Shh as far anterogradely as the superior colliculus (Traffort et al., 2001).

Here we propose and provide evidence for a model of Shh-mediated ipsilateral RGC guidance, which reconciles how Shh can guide ipsilateral RGCs at the optic chiasm in the absence of its local expression at the chiasm. Crucially, our model postulates that Shh is not present at the optic chiasm prior to the arrival of RGCs but is instead synthesized and transported by contralateral RGC axons, accumulating at the chiasm and repelling subsequent ipsilateral RGCs, which arrive later at the optic chiasm. By demonstrating that RGC-derived Shh acts trans-axonally to guide the ipsilateral RGC population, our results expand the current paradigm of choice point axon guidance.

RESULTS

限制

***Shh* mRNA Is Confined to the Retina while *Shh* Protein Strongly Localizes at the Optic Chiasm**

To examine how Shh acts on ipsilateral RGCs at the optic chiasm, we first sought to characterize its localization in detail by performing *in situ* hybridization and immunostainings on embryonic mouse sections. *Shh* mRNA was found in the retina, but not at the optic chiasm at embryonic day (E)15.5 (Figure 1A), agreeing with *in situ* hybridization data from previous studies (Macdonald et al., 1997; Torres et al., 1996; Trousse et al., 2001). However, while some studies have been unable to detect Shh protein at the optic nerve and chiasm using older Shh antibodies (Wallace and Raff, 1999), we successfully visualized Shh protein at the optic nerve and chiasm by immunostaining with a recently developed, sensitive polyclonal Shh antibody (Tian et al., 2009) (Figure 1B). This antibody is specific to Shh as it detects Shh at the notochord and floor plate of *Shh* heterozygote mouse embryos, but it does not give a signal in *Shh* mutant embryos (Figure S1) (Sloan et al., 2015). To eliminate the possibility that the Shh protein at the optic chiasm is translated from an earlier transient mRNA source at the chiasm, we further performed *in situ* hybridization on serial coronal mouse sections at E13.5 and E14.5, when axons first reach the chiasm (Figure 1D). Unlike *Ephrin-B2* (Williams et al., 2003) (schematized in Figure 1E), no *Shh* mRNA was found close to the optic chiasm that could plausibly explain the strong Shh protein immunoreactivity that was found concentrated at the chiasm.

Since *Shh* mRNA is confined to the RGC layer of the retina while the protein is also detected at the optic nerve and chiasm (Figure 1C), we postulated that Shh is translated at the RGC cell bodies and the protein is transported anterogradely along the axons that make up the nerve and chiasm. To examine the distribution of Shh protein along RGC axons, we quantified the intensity of Shh immunofluorescence on cross sections

of the optic nerve, optic chiasm, and optic tract at E15.5, during the peak phase of axon growth at the optic chiasm (Petros et al., 2008). Interestingly, while we observed Shh immunofluorescence along the axons as far anterogradely as the optic tract, the signal peaked at the optic chiasm, where it was 53% higher than the optic nerve (optic chiasm: 1.53 ± 0.06 , optic nerve: 1.00 ± 0.04 ; n = 6; p < 0.01) and 36% higher than the optic tract (optic chiasm: 1.53 ± 0.06 , optic tract: 1.17 ± 0.11 ; n = 6; p < 0.05) (Figures 1F and 1G). Thus, the mRNA and protein expression of *Shh* is consistent with our hypothesis that retina-derived Shh is transported anterogradely by RGC axons to the optic chiasm, a site of high Shh accumulation.

电穿孔

Retina-Electroporated ShhYFP Localizes Strongly to the Optic Chiasm

To further test the ability of RGCs to transport Shh to the chiasm, we electroporated an ShhYFP fusion construct into the retina of E13.5 mouse embryos to see its eventual localization at E16.5 (Figure 2A). The yellow fluorescent protein (YFP) in the construct is inserted just before the autocatalytic cleavage site of Shh, and thus the fusion protein should retain both the palmitate and cholesterol lipid modifications to mimic endogenous Shh localization (Figure 2B) (Beug et al., 2011). We co-electroporated ShhYFP with mCherry, a fluorophore that does not undergo preferential localization, as a baseline control.

When relative intensity levels for ShhYFP and mCherry were measured at the retina, optic nerve, and optic chiasm, we found a difference in the localization pattern between ShhYFP and mCherry along RGCs. Using their respective levels at the retina as a baseline, ShhYFP levels were higher than mCherry at the optic nerve (ShhYFP: 2.55 ± 0.61 , mCherry: 0.75 ± 0.18 ; n = 4; p < 0.05) and optic chiasm (ShhYFP: 3.40 ± 0.62 , mCherry: 0.81 ± 0.12 ; n = 4; p < 0.001) (Figures 2C and 2D). When ShhYFP levels were divided by mCherry levels to obtain a more accurate representation of the differential localization of ShhYFP, the ShhYFP/mCherry ratio was found to be $3.8 \times$ higher at the optic nerve than the retina (optic nerve: 3.77 ± 0.64 , retina: 1.00 ± 0.12 ; n = 4; p < 0.01) and $4.5 \times$ higher at the chiasm than the retina (optic chiasm: 4.51 ± 0.51 , retina: 1.00 ± 0.12 ; n = 4; p < 0.01) (Figure 2E). Taken together, these results suggest that RGCs preferentially transport Shh anterogradely to the optic chiasm.

Shh at the Optic Chiasm Is Produced and Transported by Earlier-Arriving Contralateral RGCs, before Ipsilateral Axons Arrive

Our data indicate that retina-derived Shh is transported by RGC axons to the optic chiasm. Based on these results, we hypothesized that Shh is synthesized and transported by contralateral RGC axons, accumulates at the chiasm, and subsequently repels later-arriving ipsilateral RGCs when they reach the optic chiasm. According to this model, contralateral, but not ipsilateral, RGCs should express Shh. Although the large majority of RGCs express Shh at E15.5, indicating that Shh is expressed by contralateral RGCs, Shh protein can also be detected in the ventrot temporal retina where ipsilateral RGCs reside (Figure 1B, asterisk). In addition to ipsilateral RGCs, this region also gives rise to contralateral RGCs in mice (Jeffery, 2001), making it difficult to determine whether ipsilateral RGCs also express Shh. To

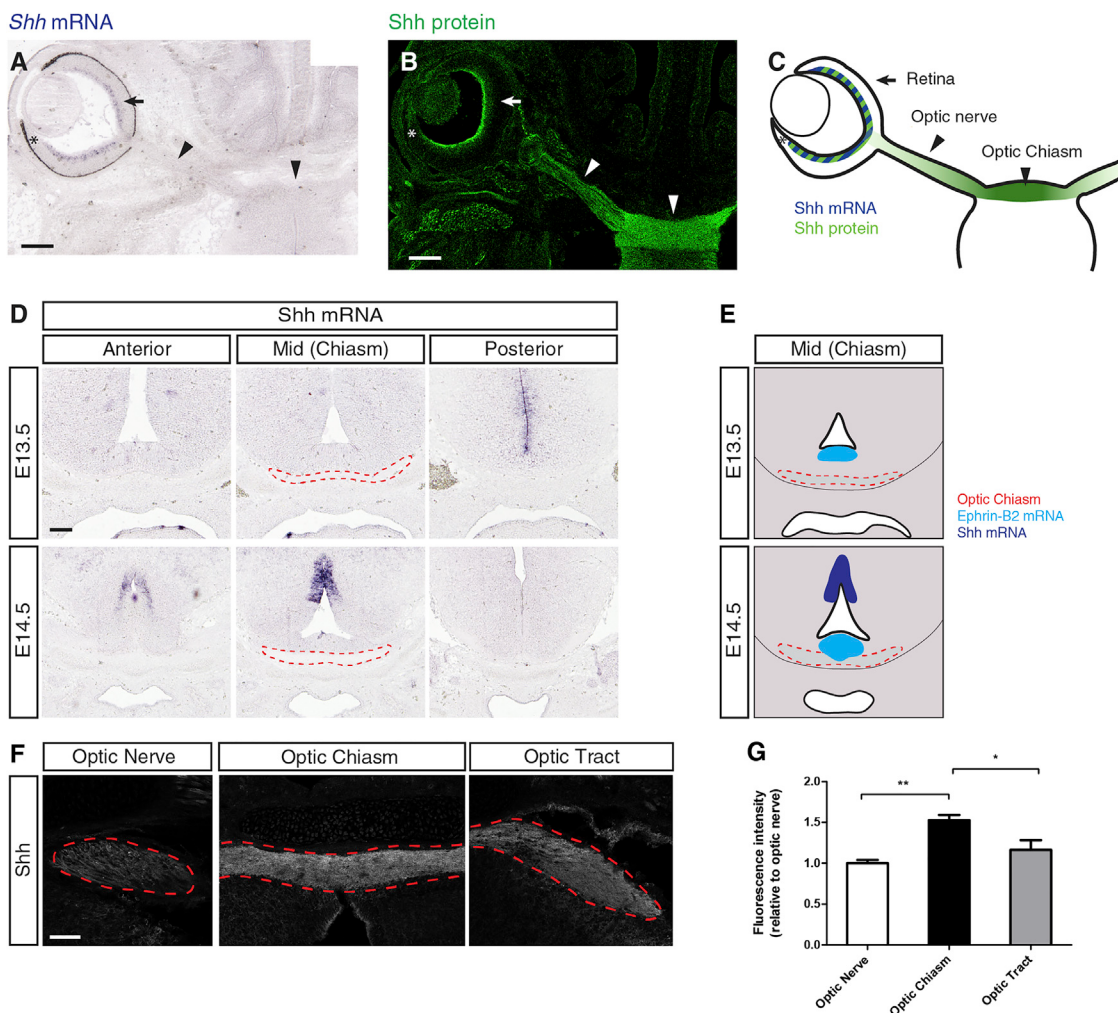


Figure 1. *Shh* mRNA Is Confined to the Retina, while *Shh* Protein Strongly Localizes at the Optic Chiasm

(A–C) *In situ* hybridization with an *Shh* probe (A) and immunofluorescence labeling with an *Shh* antibody (B) on mouse embryo E15.5 sections show *Shh* mRNA exclusively at the retina (arrow), while *Shh* protein is found at the retina (arrow), optic nerve (arrowhead), and optic chiasm (arrowhead). This expression pattern of *Shh* mRNA and protein is summarized in (C). Asterisks indicate the ventrotemporal crescent, from where ipsilateral RGCs originate.

(D) *In situ* hybridization with *Shh* probe on E13.5 and E14.5 mouse coronal serial sections, from anterior to posterior. *Shh* mRNA is found at the interior of the third ventricle and at the midline far dorsal from the optic chiasm, but never at or adjacent to the optic chiasm. Red dashed outline indicates the boundary of the optic chiasm.

(E) Schematic illustration of the location of *Shh* and *Ephrin-B2* mRNA in coronal sections of the mouse optic chiasm.

(F) Immunofluorescence labeling of *Shh* on coronal sections of RGC axons in mouse E15.5 embryos.

(G) Quantification of the average fluorescence intensity in (F), relative to intensity at the optic nerve. The *Shh* intensity is 53% higher at the chiasm compared to the optic nerve ($p < 0.01$) and 36% higher than the optic tract ($p < 0.05$) ($n = 6$; one-way repeated-measures ANOVA with Tukey's posttest, * $p < 0.05$ and ** $p < 0.01$). The intensity was quantified from 6 different embryos, using the average of 2–5 sections for each optic area. See also Figure S1. Error bars indicate SEM; n represents the number of embryos. Scale bars, 200 μ m (A, B, and D) and 50 μ m (F).

further assess this, we used an *Shh-Cre* line to genetically label *Shh*-producing cells with tdTomato, and then we immunostained with an antibody for the ipsilateral marker Zic2 (Figure 3A) (Brown et al., 2003). We next determined whether any RGCs were double-labeled at E14.5, when Zic2 expression first turns on in RGCs (Herrera et al., 2003). In the ganglion cell layer of the ipsilateral transition zone (which we defined as starting in the temporal retina at the first Zic2-expressing cell and extending 300 μ m toward the medial retina), we found that 0/86 Zic2-positive cells expressed tdTomato, while 80/168 Zic2-negative cells ex-

pressed tdTomato (Fisher's exact test, $p < 0.0001$). These results suggest that *Shh* expression is restricted to non-ipsilateral (i.e., contralateral) RGCs, which is consistent with our model that contralateral RGCs secrete *Shh* at the optic chiasm and ipsilateral RGCs respond to this contralateral RGC-derived *Shh*.

We next investigated the developmental timing of *Shh* expression in conjunction with RGC axon extension and arrival at the optic chiasm. According to our model, *Shh* at the chiasm is produced by contralateral RGCs, and the very first *Shh* expression at the optic chiasm occurs when contralateral RGCs arrive at

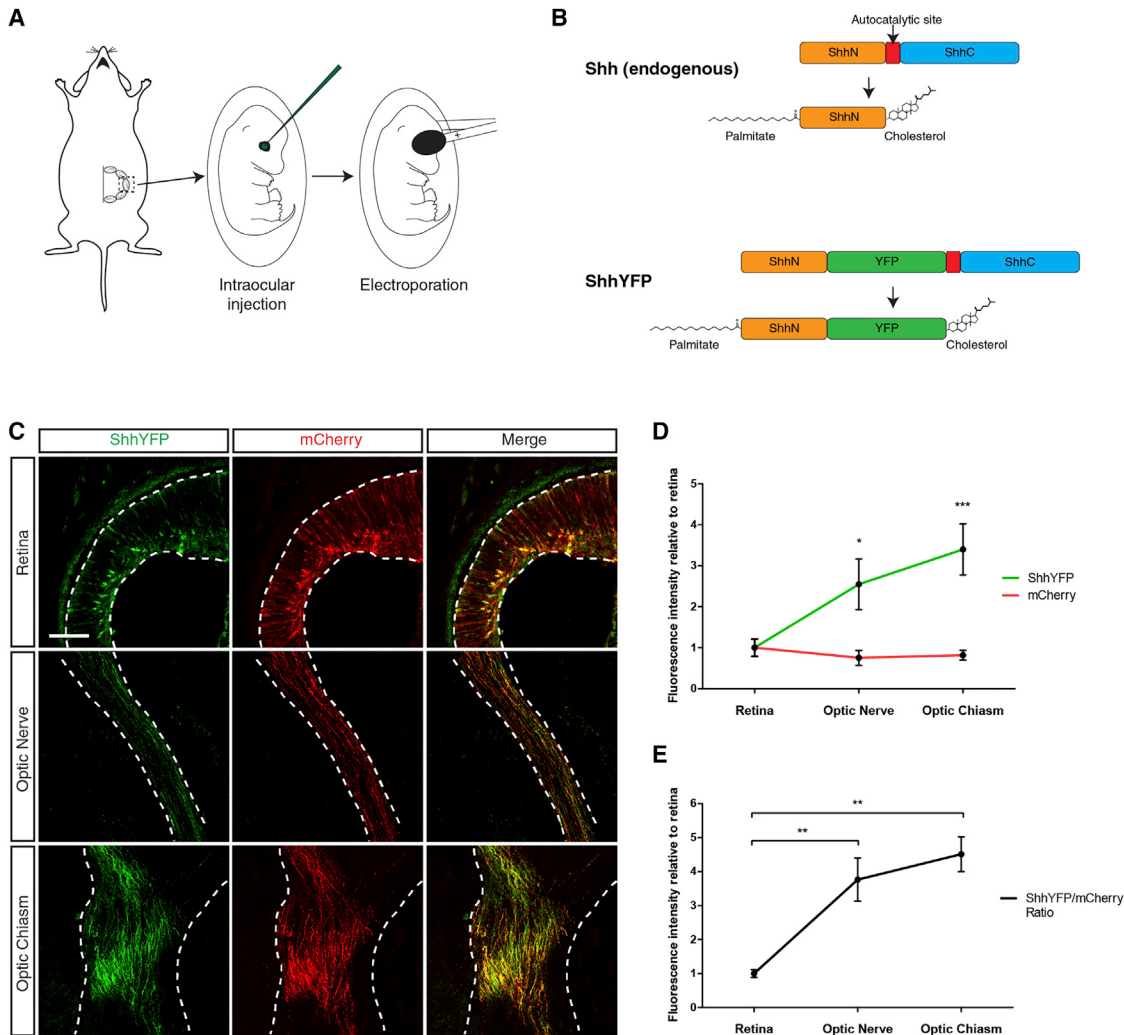


Figure 2. Retina-Electroporated ShhYFP Localizes Strongly to the Optic Chiasm

(A) Illustration of *in utero* electroporation of ShhYFP into the retina. The E13.5 embryos are exposed via ventral laparotomy of an anesthetized female. The plasmid is injected into the intraretinal space and electroporated with paddle electrodes.

(B) Schematic model of the processing of endogenous Shh and ShhYFP. Full-length unprocessed Shh undergoes autocleavage, followed by the addition of palmitate and cholesterol. In ShhYFP, YFP is inserted just before the autocleavage site, and the processed ShhYFP retains both lipid modifications.

(C) Immunofluorescence images of horizontal E15.5 mouse embryo sections that have been co-electroporated in the retina with ShhYFP and mCherry expression vectors at E13.5. Antibodies against GFP and mCherry were used to enhance the detection of ShhYFP and mCherry.

(D) Quantification of the average fluorescence intensity of ShhYFP and mCherry in areas shown in (C), relative to the retina. The intensity of ShhYFP is higher than mCherry at the optic nerve (ShhYFP: 2.55 ± 0.61 , mCherry: 0.75 ± 0.18 ; $n = 4$; $p < 0.05$) and optic chiasm (ShhYFP: 3.40 ± 0.62 , mCherry: 0.81 ± 0.12 ; $n = 4$; $p < 0.001$) ($n = 4$; two-way repeated-measures ANOVA with Bonferroni posttest, * $p < 0.05$ and *** $p < 0.001$).

(E) Quantification of the ShhYFP/mCherry average fluorescence intensity ratio seen in (D). Compared to the retina, the ShhYFP/mCherry ratio is $3.8 \times$ higher in the optic nerve ($p < 0.01$) and $4.5 \times$ higher in the optic chiasm ($p < 0.01$) ($n = 4$; one-way repeated-measures ANOVA with Tukey's posttest, ** $p < 0.01$). Quantifications from four electroporated embryos were included in the analysis. Error bars indicate SEM; n represents the number of embryos. Scale bar, 100 μ m.

the chiasm. Therefore, Shh should be absent from the presumptive optic chiasm area prior to RGC axon arrival. We thus examined Shh protein expression at E12.5, a stage when RGC axons have not yet reached the optic chiasm (Figure 3B, top). At this stage, we could already see Shh expression in the retina and the optic nerve in Tag1-positive RGC axons (Chatzopoulou et al., 2008) (Figure 3B, arrow), but we did not detect Shh at the optic chiasm (Figure 3B, bottom). It was not until E13.5 that Shh was detected at the optic chiasm, coinciding with the arrival of Tag1-

positive RGC axons at the optic chiasm (Figure 3C). This suggests that Shh at the chiasm is derived from contralateral RGC axons.

We next examined whether ipsilateral RGCs arrive at the chiasm after contralateral RGCs, so that Shh expression is already established by earlier-arriving contralateral axons to repel later-arriving ipsilateral axons. To examine the timing of ipsilateral axon arrival, we used an ipsilateral RGC-specific Cre mouse line (*Sic6a4-Cre*) (Koch et al., 2011) to selectively label ipsilateral RGCs with the fluorescent tdTomato marker

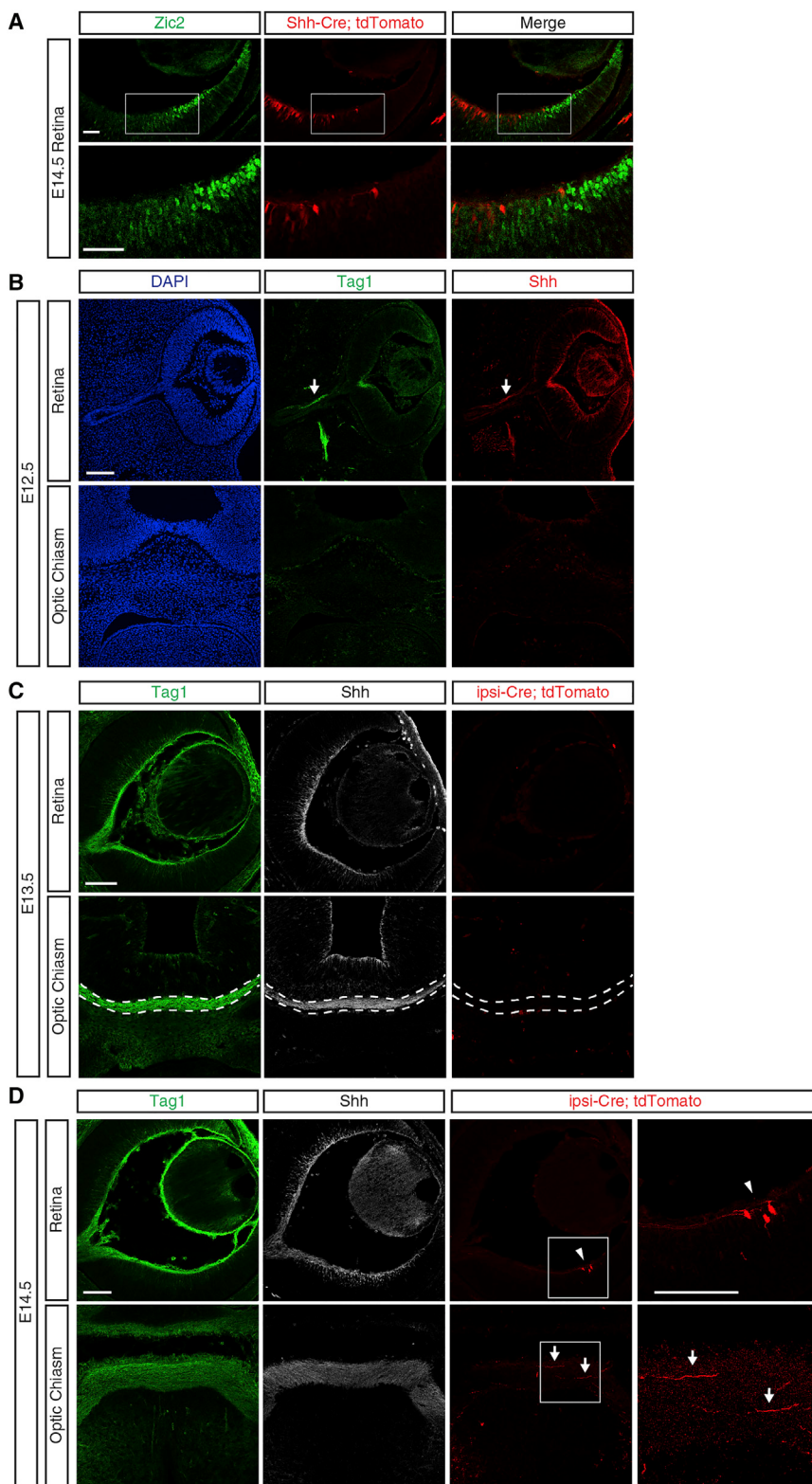


Figure 3. Shh at the Optic Chiasm Is Produced and Transported by Earlier-Arriving Contralateral RGCs, before Ipsilateral Axons Arrive

(A) Coronal section of an E14.5 *Shh-Cre; tdTomato* retina immunolabeled with a Zic2 antibody. White boxes indicate the enlarged areas shown in the bottom row images. Zic2-positive cells and *tdTomato*-positive cells are mutually exclusive, suggesting that ipsilateral RGCs do not express Shh.

(B) Coronal sections of wild-type E12.5 embryos immunolabeled with DAPI, the RGC axon marker Tag1, and Shh. At E12.5, RGC axons have not yet reached the optic chiasm. However, Shh is already expressed in the retina and optic nerve (top, arrow). Optic chiasm sections (bottom) show the absence of Shh expression and RGC axons.

(C and D) Coronal sections of *ipsi-Cre; tdTomato* E13.5 and E14.5 embryos immunolabeled with the RGC axon marker Tag1, Shh, and anti-dsRed to enhance the *tdTomato* marker. At E13.5 (C), Tag1-positive RGC axons have reached the optic chiasm (white dashed outline) and express Shh. However, no *tdTomato*-positive neurons are detected in the retina or optic chiasm, indicating that the first axons to reach the optic chiasm are contralateral RGCs. At E14.5 (D), the first *ipsi-Cre; tdTomato*-positive cell bodies and axons are detected in the retina (arrowhead) and optic chiasm (arrows). White squares indicate the enlarged areas. In (C) and (D), the Tag1 and *ipsi-Cre; tdTomato* panels display the same tissue section, while the Shh panel displays an adjacent serial section of the same embryo. See also Figure S2. Scale bars, 50 μm (A) and 100 μm (B–D).

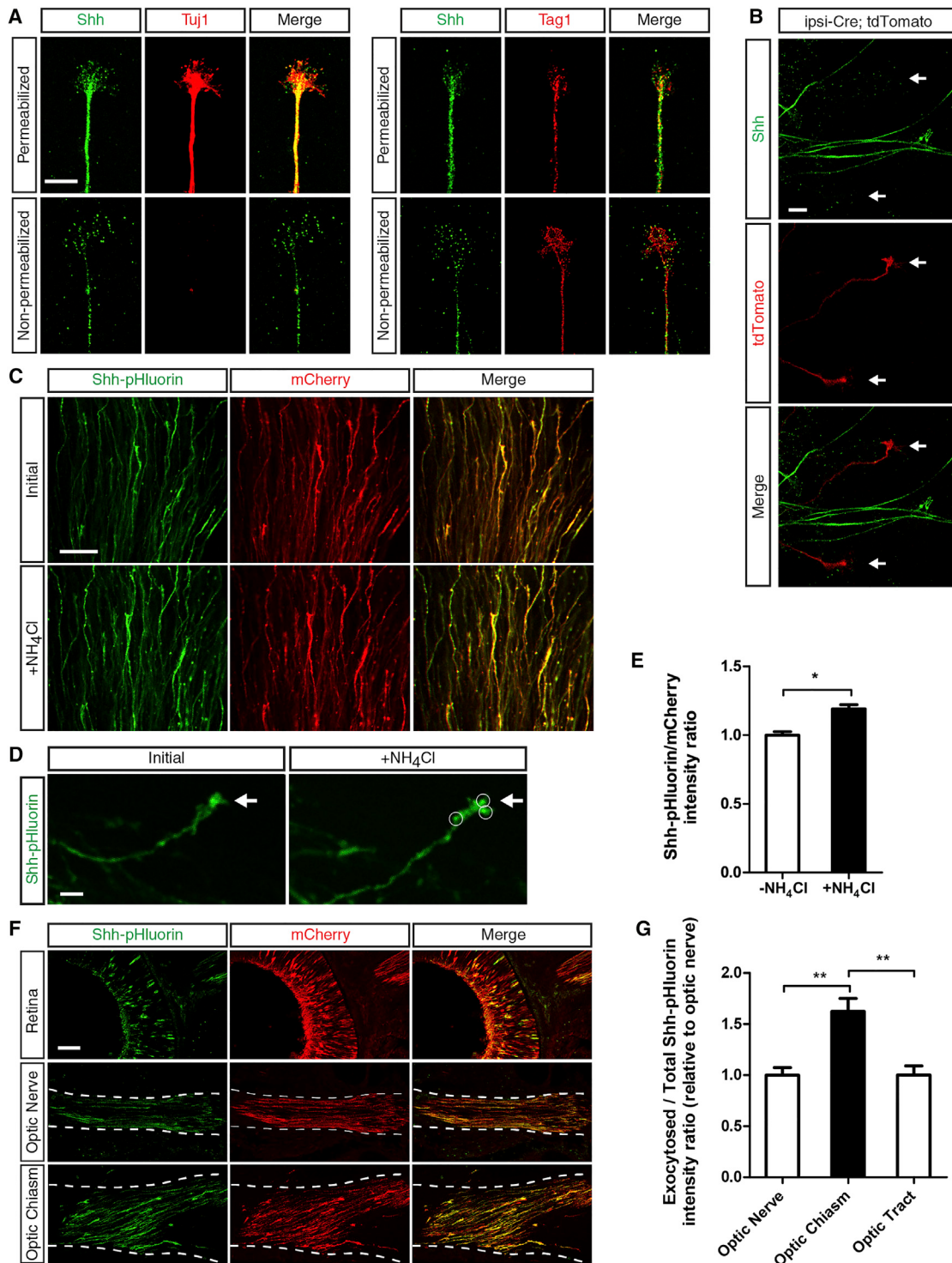


Figure 4. Shh Is Secreted by Contralateral RGC Axons *In Vitro* and Preferentially Secreted at the Optic Chiasm *In Vivo*

(A) Immunofluorescence labeling of Shh, Tuj1, and Tag1 on RGC explants cultured for 10 hr from E16.5 mouse embryo retina, under permeabilizing and non-permeabilizing conditions. Puncta of Shh can be detected along the axon and growth cone in non-permeabilizing conditions, indicating it is secreted by RGC axons.

(B) Immunofluorescence labeling of Shh in RGC explants cultured for 10 hr from *Slc6a4-cre; tdTomato* E16.5 mouse retina under permeabilizing conditions. Arrows point to *Slc6a4-Cre*-positive ipsilateral RGCs, which do not express Shh.

(legend continued on next page)

(ipsi-Cre; tdTomato). At E13.5, although Tag1 staining showed RGC axons present at the optic chiasm, no tdTomato-positive cell body or axon could be detected in the retina and optic chiasm, suggesting that all RGC axons at the optic chiasm at this stage are contralateral (Figure 3C). Also, Shh immunolabeling revealed that Shh protein expression at the chiasm was already established prior to the arrival of tdTomato-positive ipsilateral axons. It was not until E14.5 that we saw the first tdTomato-positive RGC cell bodies and axons in the retina and optic chiasm (Figure 3D, box), corresponding with the beginning of expression of Zic2, the ipsilateral transcription factor responsible for conferring ipsilateral identity (Herrera et al., 2003). Furthermore, we confirmed that the Boc receptor, which is required for responsiveness to Shh repulsion, was expressed by ipsilateral RGCs at E14.5, a time when they first reach the optic chiasm (Figure S2). Altogether, these results are consistent with our hypothesis that Shh at the optic chiasm is produced and transported by earlier-arriving contralateral RGCs to repel later-arriving ipsilateral axons trans-axonally.

Shh Is Secreted by Contralateral RGCs at the Optic Chiasm

Transport of Shh to the optic chiasm is not sufficient for Shh to act as a guidance cue on ipsilateral RGCs at the optic chiasm; Shh must also be secreted. We first tested whether RGCs secrete Shh *in vitro* by performing immunostaining of E16.5 RGC explants in non-permeabilizing conditions. Under these conditions, in which intracellular tubulin (Tuj1) could not be detected, we found Shh puncta along both the axon and growth cone, in a fashion similar to Tag1, an extracellular neuronal adhesion molecule expressed by RGCs (Figure 4A).

Next, we verified *in vitro* whether Shh is produced and secreted by the contralateral RGC population exclusively. We again took advantage of the ipsilateral RGC-specific Cre mouse to label ipsilateral RGCs with tdTomato (ipsi-Cre; tdTomato), and we performed Shh immunostaining on retina explants made from that line (Figure 4B). We found that 0/15 of examined ipsilateral axons expressed Shh, while conversely 23/26 of examined contralateral axons expressed Shh (Fisher's exact test, $p < 0.0001$), indicating that contralateral, but not ipsilateral, RGCs produce Shh, consistent with what we found *in vivo* (Figure 3A). These results agree with and expand on previous studies that detected Shh in RGCs cultured from the dorsonasal retina, but not the ventrotemporal retina, from where ipsilateral RGCs originate (Sánchez-Camacho and Bovolenta, 2008). Furthermore, our results support our hypothesis that contralat-

eral RGCs are the producers of Shh while ipsilateral RGCs respond to the contralateral RGC-derived Shh.

To determine whether Shh is secreted by RGCs at the optic chiasm *in vivo*, we made use of superecliptic pHluorin, a pH-sensitive GFP variant that loses fluorescence in low pH environments (Sankaranarayanan et al., 2000). It is commonly used when studying exocytosis and surface localization of proteins, since proteins tagged with superecliptic pHluorin are not fluorescent inside acidic vesicles prior to exocytosis and only become fluorescent once exocytosed into the pH-neutral extracellular environment (Ashby et al., 2004). Thus, we performed *in utero* electroporation of Shh-pHluorin and mCherry into the retina at E13.5 to examine the secretion of Shh both *ex vivo* and *in vivo* (Figures 4C–4G). First, we dissected the entire optic chiasm along with a portion of the optic nerve from electroporated E16.5 embryos, and we immediately imaged the fresh tissue whole-mount preparation with a spinning-disk confocal microscope. We detected a robust Shh-pHluorin signal along the entirety of most electroporated axons and growth cones (Figure 4C), indicating that Shh is strongly exocytosed by RGC axons at the chiasm. As a control, we then immersed the chiasm tissue in 50 nM NH₄Cl to neutralize acidic intracellular vesicles, which renders intracellular Shh-pHluorin fluorescent (Miesenböck et al., 1998). The addition of NH₄Cl revealed some previously undetected puncta of Shh-pHluorin, likely intracellular vesicles (Figure 4D), as well as an increase in the overall Shh-pHluorin intensity (Figure 4E). In addition, we sectioned fixed E16.5 heads, and we detected the pHluorin signal at the retina, optic nerve, and strongly at the optic chiasm, in agreement with our hypothesis (Figure 4F). Importantly, quantification of the exocytosed Shh-pHluorin signal over the total Shh-pHluorin signal (exocytosed + intracellular, detected by immunolabeling with a GFP antibody) revealed that Shh is preferentially secreted at the chiasm, compared to the optic nerve and optic tract (Figure 4G). Taken together, these results indicate that Shh is indeed secreted by RGCs and that a significant amount of this secretion occurs at the chiasm.

Ipsilateral RGCs Are Repelled by Contralateral RGCs *In Vitro* in a Boc- and Smo-Dependent Manner

Since we could detect Shh extracellularly along axons of contralateral RGCs *in vitro* (Figure 4A), we wondered whether this Shh can repel ipsilateral RGC growth cones in a live culture. To answer this question, we performed time-lapse imaging of RGC explants from E16.5 ipsi-Cre; tdTomato retina 10 hr after dissection and plating (Figure 5A). Using the tdTomato marker

(C) Confocal images of an intact E16.5 optic chiasm preparation electroporated with Shh-pHluorin and mCherry at E13.5 (top). The optic chiasm preparation was then immersed and remounted in PBS with 50 nM NH₄Cl and re-imaged (bottom).

(D) Close-up of an axon from an intact E16.5 optic chiasm preparation before and after immersion in NH₄Cl. After treatment with NH₄Cl, which neutralizes acidic vesicles, puncta of Shh vesicles were detected in the growth cone (arrow).

(E) Quantification of the relative Shh-pHluorin and mCherry fluorescence intensities of RGC axons in the intact optic chiasm preparation, before and after the addition of 50 nM NH₄Cl. The addition of NH₄Cl led to a 19% increase in the level of Shh-pHluorin compared to mCherry ($n = 4$; paired two-tailed t test, $*p = 0.04$). n represents the number of optic chiasm preparations analyzed.

(F) Horizontal sections of E15.5 mouse embryos co-electroporated with Shh-pHluorin and mCherry in the retina at E13.5. Shh-pHluorin can be detected strongly at the optic chiasm.

(G) Quantification of the intensity ratio of exocytosed versus total Shh-pHluorin, relative to the ratio at the optic nerve. The exocytosed/total Shh-pHluorin ratio is 1.6× higher at the optic chiasm compared to the optic nerve or optic tract ($n = 5$; one-way repeated-measures ANOVA with Tukey's posttest, $**p < 0.01$). Error bar indicates SEM; n represents the number of embryos. Scale bars, 10 μm (A, B, and D), 50 μm (C), and 100 μm (F).

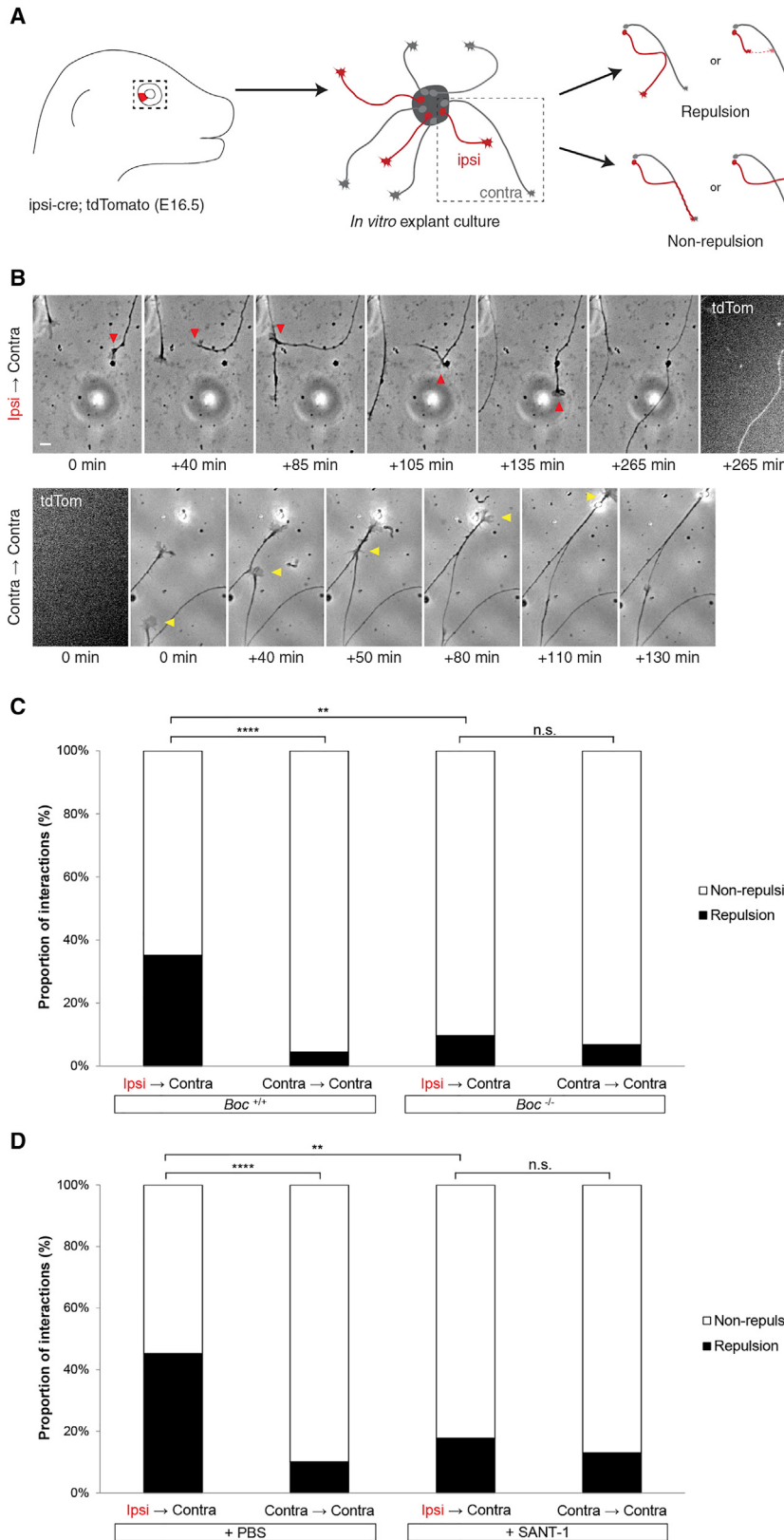


Figure 5. Ipsilateral RGCs Are Repelled by Contralateral RGCs In Vitro in a *Boc*- and *Smo*-Dependent Manner

(A) Schematic of the *in vitro* RGC axon-axon interaction assay. Retina explants were made from *Slc6a4cre*; *tdTomato* E16.5 animals to identify ipsilateral RGCs, and time-lapse imaging of explants started 10 hr later. Instances of an ipsilateral growth cone encountering a contralateral axon (including growth cone) were identified, and the interaction was scored as a repulsive (the growth cone turned away or retracted) or non-repulsive interaction (the growth cone grew past the axon or fasciculated with the axon).

(B) Sample time-lapse images of an interaction between an ipsilateral growth cone and contralateral axon resulting in retraction (top) and an interaction between a contralateral growth cone and contralateral axon resulting in fasciculation (bottom). These time-lapse examples are also shown in [Movies S1](#) and [S2](#).

(C) Quantification of the axon-axon interactions observed in RGC explants on a *Boc* wild-type versus mutant background. On a wild-type background, contralateral axons selectively repel ipsilateral growth cones, but not contralateral growth cones (ipsi-contra: 35.1% [13/37 repulsion], contra-contra: 4.4% [3/68 repulsion]; $n = 37$ and 68; Fisher's exact test, $p < 0.0001$). This selective repulsive response was lost when the experiment was performed on a *Boc*^{-/-} background (ipsi-contra: 9.8% [6/62 repulsion], contra-contra: 6.8% [5/74 repulsion]; $n = 62$ and 74; Fisher's exact test, n.s.). Ipsilateral growth cones lacking the *Boc* receptor showed lower repulsion by contralateral axons compared to wild-type ipsilateral growth cones (*Boc*^{-/-}: 9.8% [6/62 repulsion], wild-type: 35.1% [13/37 repulsion]; $n = 62$ and 37; Fisher's exact test, $p = 0.0028$). At least 37 interactions were scored for each group.

(D) Quantification of axon-axon interactions observed in RGC explants with either PBS or SANT-1 added to the culture media. With PBS treatment, ipsilateral growth cones are selectively repelled by contralateral axons when compared to contralateral growth cones (ipsi-contra: 45.2% [19/42 repulsion], contra-contra: 10.1% [8/79 repulsion]; $n = 42$ and 79; Fisher's exact test, $p < 0.0001$). This selective repulsive response was lost when the *Smo* inhibitor SANT-1 was added prior to time-lapse imaging (ipsi-contra: 17.7% [8/45 repulsion], contra-contra: 13.0% [9/69 repulsion]; Fisher's exact test, n.s.). Ipsilateral growth cones treated with SANT-1 had diminished repulsive responses toward contralateral axons compared to control ipsilateral growth cones (SANT-1: 17.7% [8/45 repulsion], PBS: 45.2% [19/42 repulsion]; $n = 45$ and 42; Fisher's exact test, $p < 0.01$). At least 42 interactions were scored for each group. See also [Figure S2](#) and [Movies S1](#) and [S2](#). ** $p < 0.01$ and *** $p < 0.0001$. n represents the number of interactions. Scale bar, 10 μ m.

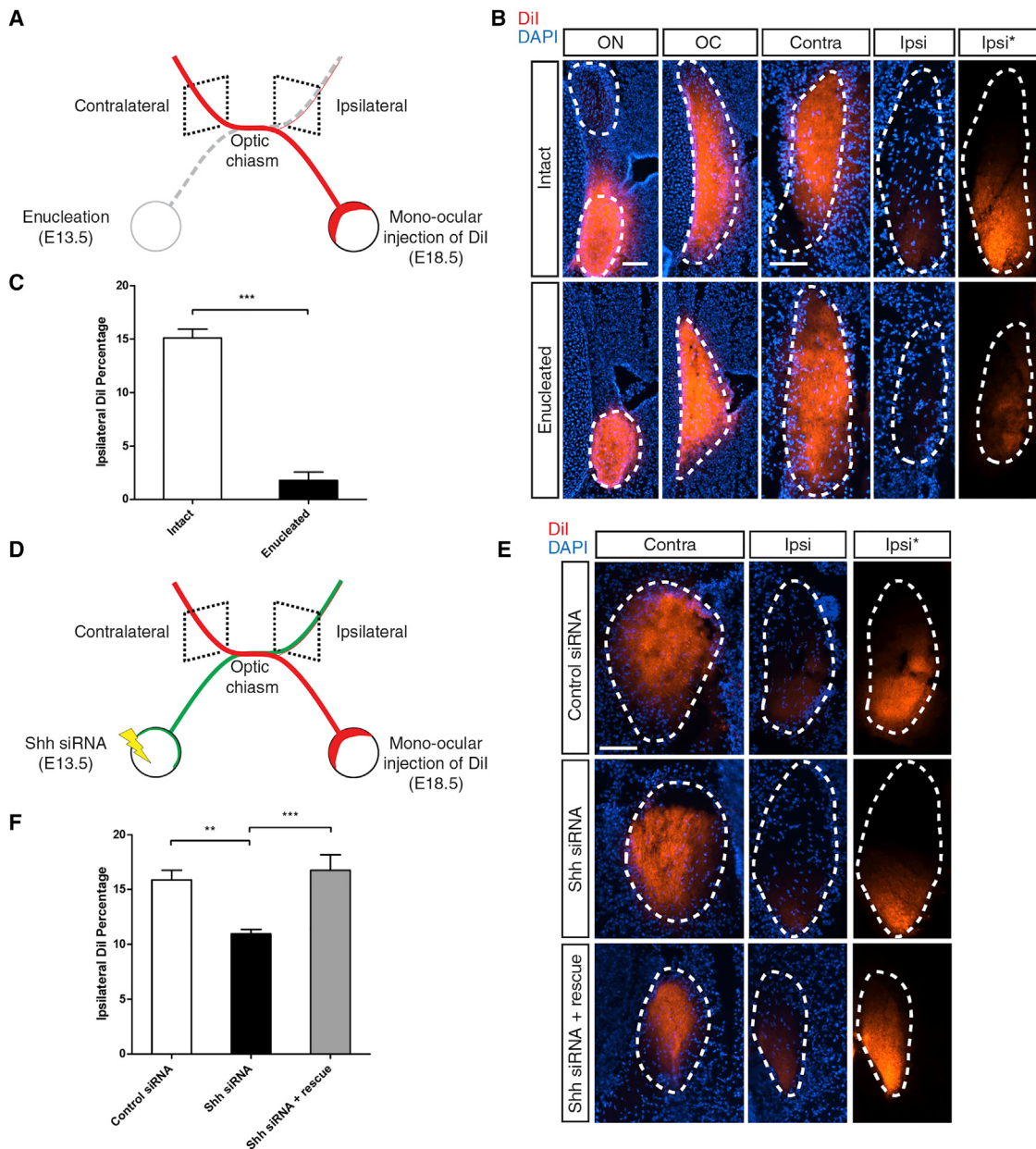


Figure 6. Knockdown of Shh in the Retina Lowers the Proportion of Ipsilateral Axons in a Non-Cell-Autonomous Manner

(A) Schematic of the experimental setup to assess the effect of enucleation on ipsilateral segregation *in vivo*. First, monocular enucleation was performed on an E13.5 mouse embryo *in utero*. Then, at E18.5, the embryo was collected and Dil was placed in the intact eye and allowed to diffuse for 2 weeks. Coronal sections were collected to assess the relative Dil fluorescence level between the ipsilateral and contralateral tracts.

(B) Representative coronal sections from enucleated and control E18.5 mouse embryos labeled with Dil as described in (A). The DAPI signal was used to identify boundaries of the optic nerve, chiasm, and tract, indicated by the white dashed lines. The Ipsi column images are brightened 4× in the Ipsi* column for better visibility. In enucleated animals, the non-labeled optic nerve (ON) is not observed and the optic chiasm (OC) is smaller.

(C) Quantification of the ipsilateral Dil intensity as a percentage of total (ipsi + contra) intensity, measured as the sum intensity of the encircled optic tract. In enucleated embryos, the remaining eye showed a reduction in ipsilateral Dil percentage compared to intact control embryos (enucleated: 1.8% ± 0.8%, intact: 15.1% ± 0.8%; n = 4; Student's two-tailed t test, p < 0.0001). Data points from 4 embryos are included in each condition.

(D) Schematic of the experimental setup to assess the effect of Shh knockdown on ipsilateral segregation *in vivo*. First, siRNA against Shh was electroporated into one eye of an E13.5 mouse embryo *in utero*. At E18.5, the embryo was collected and Dil was placed in the opposite, non-electroporated eye and allowed to diffuse for 2 weeks. Coronal sections were collected to assess the relative Dil fluorescence level between the ipsilateral and contralateral tracts.

(E) Representative images of coronal sections of a Dil-traced E18.5 embryo described in (D), stained with DAPI. Boundaries of the optic tract are indicated by the white dashed line. The Ipsi column images are brightened 4× in the Ipsi* column for better visibility.

(legend continued on next page)

to identify ipsilateral RGCs, we examined instances where an ipsilateral growth cone grew toward a contralateral axon, and we noted the outcome of every interaction. The interactions were scored as repulsion or non-repulsion, with repulsion including instances where the growth cone sharply turned away or retracted upon contacting the contralateral axon and non-repulsion including instances where the ipsilateral growth cone fasciculated with the contralateral axon or passed through unhindered (Figure 5A). We then compared the responses made by ipsilateral growth cones to those made by contralateral growth cones. Examples of interactions between ipsi-contra and contra-contra growth cones and axons are shown in Figure 5B, and time-lapse movies are also provided (Movies S1 and S2).

Quantification of these interactions demonstrated that ipsilateral growth cones were 8 times more likely than contralateral growth cones to exhibit repulsive responses when contacting a contralateral axon (ipsi-contra: 35.1%, contra-contra: 4.4%; n = 37 and 68; p < 0.0001) (Figure 5C). Since the Shh receptor Boc is expressed exclusively by ipsilateral RGCs (Figure S2; Fabre et al., 2010), this result is consistent with a model where Shh secreted by contralateral RGCs acts on the Boc receptor on ipsilateral RGCs to cause repulsion. To test this hypothesis, we performed the experiment in a *Boc* mutant background, where the ipsilateral RGCs lack the Boc receptor. We found that the *Boc* mutation caused ipsilateral growth cones to lose their repulsive response when contacting contralateral axons (*Boc*^{-/-}: 9.8%; *Boc*^{+/-}: 35.1%; n = 37 and 62; p < 0.0028). Furthermore, in a *Boc*^{-/-} background, there was no longer a difference between the responses of ipsilateral and contralateral growth cones when contacting contralateral axons (ipsi-contra: 9.8% repulsion, contra-contra: 6.8%; n = 62 and 74; not significant [n.s.]). Therefore, ipsilateral RGCs require Boc to be repelled by contralateral RGCs.

We previously showed that bath application of Shh induces collapse of Boc-positive growth cones in RGC explants in a Smoothened (Smo)-dependent manner (Fabre et al., 2010). Thus, we investigated whether the repulsion of ipsilateral growth cones by contralateral axons is Smo dependent. When the Smo antagonist SANT-1 was added to our time-lapse culture, the ipsilateral growth cones lost their repulsive response to contralateral axons compared to the control (SANT-1: 17.8%, PBS: 45.2%; n = 42 and 45; p = 0.0135). Furthermore, the difference between ipsi-contra and contra-contra responses in the PBS control (ipsi-contra: 45.2%, contra-contra: 10.1%; n = 42 and 79; p < 0.0001) was abolished with the addition of SANT-1 (ipsi-contra: 17.8%, contra-contra: 13.0%; n = 45 and 69; n.s.). Therefore, Smo activity is required for ipsilateral RGCs to be repelled by contralateral RGCs.

Together, our experiments show that ipsilateral growth cones are repelled by contralateral axons *in vitro* in a Boc- and

Smo-dependent manner. Given that our immunostaining revealed the presence of Shh on the surface of contralateral axons, a mechanistic explanation for these results is that Shh at the surface of contralateral axons binds to the receptor Boc on ipsilateral growth cones to repel ipsilateral RGCs via activation of the signaling mediator Smo.

Knockdown of Shh in the Retina Reduces the Proportion of Ipsilateral Axons in a Non-cell-autonomous Manner

Our *in vitro* data showing that contralateral RGC axons secrete Shh and repel ipsilateral RGCs support an *in vivo* model where ipsilateral RGCs are repelled by contralateral RGC-derived Shh at the optic chiasm. Since our data indicate that the Shh protein at the optic chiasm is RGC derived, manipulations of Shh levels at the retina should affect Shh levels at the optic chiasm, which in turn should affect the guidance of Boc-expressing RGCs that are normally repelled away from the chiasm and project ipsilaterally. One manipulation is monocular enucleation, which removes an entire eye and thus should reduce Shh levels at the optic chiasm by half. With lower Shh levels, repulsion of normally ipsilateral-projecting RGCs should weaken and result in their misprojection to the contralateral side, thus decreasing the proportion of ipsilateral RGCs.

To test this, we performed monocular enucleation of E13.5 embryos. We then measured the ipsilateral RGC proportion by monocular Dil tracing of the remaining eye at E18.5, followed by quantification of the Dil intensity in cross sections of the contralateral and ipsilateral optic tract (Figures 6A–6C). We found a strong reduction in ipsilateral proportion in enucleated animals compared to intact controls (enucleated: 1.8% ± 0.8%, intact: 15.1% ± 0.8%; n = 4; p < 0.0001). This finding corresponds to past enucleation studies performed in various species and using different methods to estimate the ipsilateral proportion, which all show a decrease following early enucleation (Chan et al., 1999; Godement et al., 1987; Guillery, 1989). However, in addition to reduced repulsion of ipsilateral axons due to reduced levels of Shh, the drastic reduction we observed in ipsilateral RGC proportion following enucleation could also be explained by the loss of the contralateral optic tract, which would normally serve as a fasciculation target for ipsilateral RGCs (Chung et al., 2004; Dai et al., 2013; Demyanenko and Maness, 2003; Marcos et al., 2015). Furthermore, enucleation may influence the development of chiasm cells, which could disrupt expression of other known chiasm cues such as Ephrin-B2, NrCAM, Sema6D, and VEGF164 (Erskine et al., 2011; Kuwajima et al., 2012; Lustig et al., 2001; Williams et al., 2003).

To specifically manipulate Shh levels at the optic chiasm without disrupting the optic tracts and development of the optic chiasm, we unilaterally electroporated Shh-targeting small interfering RNAs (siRNAs) into the E13.5 retina, and we assessed the

(F) Quantification of the ipsilateral Dil intensity as a percentage of total (ipsi + contra) intensity, measured as the sum intensity of the encircled optic tract. The retinas of embryos electroporated with *Shh* siRNA in the opposite eye showed a reduction in ipsilateral Dil percentage compared to those electroporated with a control siRNA (control: 15.9% ± 0.9%, *Shh*: 11.0% ± 0.4%; n = 5 and 11; one-way ANOVA with Tukey's posttest, **p < 0.01) or *Shh* siRNA with an *Shh* siRNA-resistant rescue construct (*Shh*: 11.0% ± 0.4%, rescue: 16.7% ± 1.4%; n = 11 and 6; one-way ANOVA with Tukey's posttest, ***p < 0.001). Data points from 5 control siRNA, 11 *Shh* siRNA, and 6 *Shh* siRNA + rescue embryos are included, averaged from at least 3 sections per embryo. See also Figures S3 and S4. Error bars indicate SEM; n represents the number of embryos. ***p < 0.0001 and **p < 0.001. Scale bar, 100 μm.

?

单眼去核

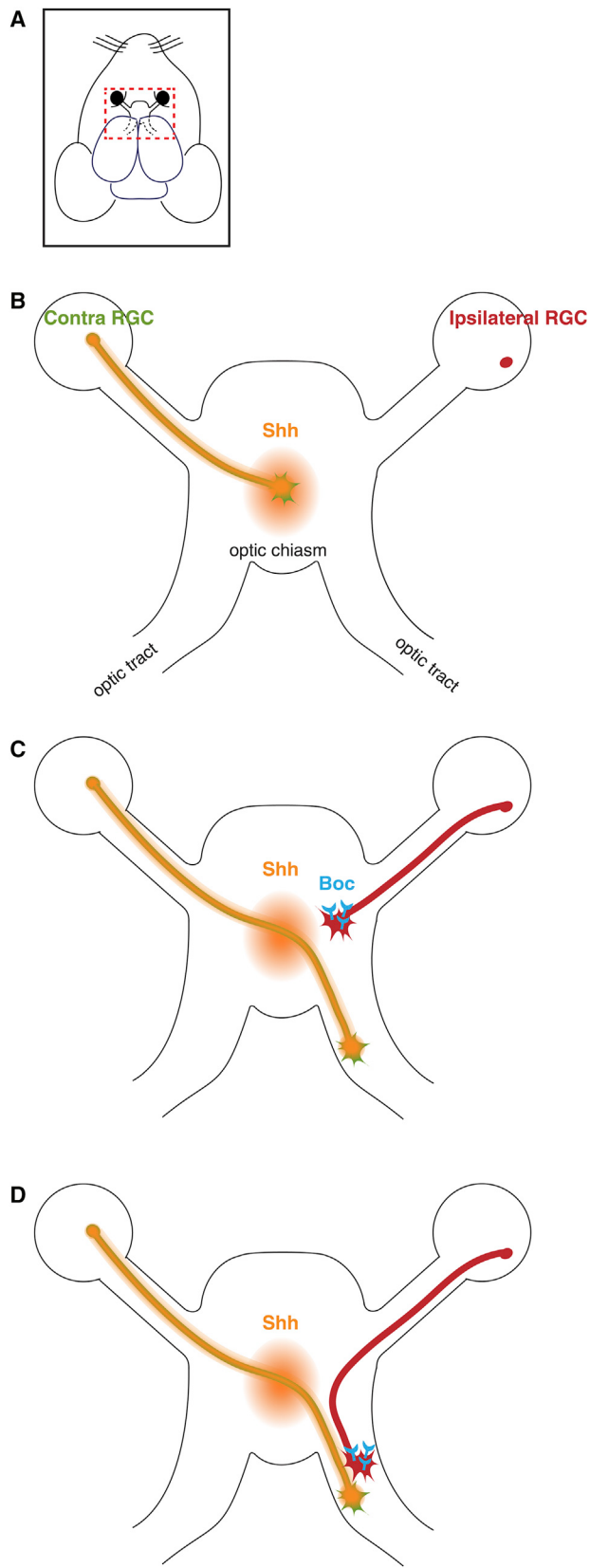


Figure 7. A Model for the Trans-axonal Guidance of Ipsilateral RGCs

(A) Schematic of the horizontal view of the mouse chiasm shown in (B)–(D). (B) Shh is produced by contralateral RGC cell bodies of the retina and transported anterogradely down the axon and secreted strongly at the optic chiasm.

(C and D) Later-arriving ipsilateral RGCs encounter this axon-derived Shh (C), and they are repelled from the midline into the ipsilateral optic tract (D). Note that the model only shows one set of contra- and ipsilateral RGCs for clarity, but this mechanism is mirrored on the opposite side.

effect by Dil tracing the other eye at E18.5 (Figures 6D and 6E). We verified that our *Shh* siRNAs were efficient in knocking down endogenous *Shh* protein from RGCs, both *in vitro* and *in vivo* (Figures S3A–S3D). We also confirmed that knockdown of *Shh* did not disrupt RGC specification, as measured by cell counts with *Brn3b*, an RGC marker (Badea et al., 2009) (Figures S3E and S3F). Compared to electroporation of a control siRNA, *Shh* siRNA resulted in a decrease in ipsilateral proportion (control: $15.9\% \pm 0.9\%$, *Shh*: $11.0\% \pm 0.4\%$; $n = 5$ and 11; $p = 0.01$) (Figure 6F). This *Shh* siRNA phenotype was rescued by the co-electroporation of an siRNA-resistant *Shh* construct (*Shh*: $11.0\% \pm 0.4\%$, *Shh* + rescue: $16.7\% \pm 1.4\%$; $n = 11$ and 6; $p < 0.001$). Notably, since knockdown of *Shh* in one eye caused a reduction in the ipsilateral proportion of the other eye, the knockdown effect was non-cell autonomous. These results support our model that *Shh* secreted by contralateral RGCs at the optic chiasm acts on ipsilateral RGCs to repel them in a non-cell-autonomous manner.

DISCUSSION

Previous studies of *Shh* expression have presented a challenge in understanding its role as a guidance cue at the optic chiasm choice point where, notably, *Shh* mRNA is absent. In our current study, we expand the prototypical model for choice point axon guidance, and we propose that remotely produced, contralateral RGC-derived *Shh* repels ipsilateral RGCs at the optic chiasm trans-axonally (Figure 7). Based on the localization and transport of endogenous *Shh* and electroporated *ShhYFP*, combined with examination of *Shh* expression and RGC axon extension at early stages, we conclude that *Shh* protein is not present at the optic chiasm prior to the arrival of RGCs. Instead, it is produced by contralateral RGCs in the retina and transported to the optic chiasm, where it is preferentially secreted and accumulates to repel later-arriving ipsilateral axons. Our time-lapse imaging of RGC interactions *in vitro*, combined with the *in vivo* effects of *Shh* knockdown in the retina, supports the model that this secreted *Shh* can specifically repel ipsilateral RGCs.

The role of axon-axon interactions has long been known to be important in proper axon growth during development, including RGCs. For example, pioneer axons can serve as guides for later axons to fasciculate onto (Soares and Mason, 2015), and cell adhesion molecules, such as NrCAM, NCAM, and L1, are expressed on the membranes of RGC axons and play a role in fasciculation of the optic nerve and tract (Chung et al., 2004; Dai et al., 2013; Demyanenko and Maness, 2003). In this study, we report for the first time an axon-axon interaction that plays a major role in determining a binary outcome at a midline choice point.

Consolidation of Shh's Localization and Function

Before the discovery of Shh as a guidance molecule, much attention was placed on its role as a morphogen, and its mRNA localization during development was scrutinized in the context of its patterning activity. Early studies on the role of Shh in the visual system came from two areas of investigation: those examining the midline region near the optic chiasm and those examining the retina.

Studies of the midline found *Shh* mRNA dorsal and ventral to the optic chiasm in embryos of different species, including E13.5 mouse, but absent at the optic chiasm itself (Macdonald et al., 1997; Torres et al., 1996; Trousse et al., 2001). Along with *in vitro* experiments showing that Shh inhibits RGC growth (Kolpak et al., 2005; Trousse et al., 2001), *in vivo* Shh overexpression experiments led to the hypothesis that Shh acts as a repulsive border that constrains growth of all RGCs and helps define the location of the optic chiasm (Trousse et al., 2001). However, as these experiments involved overexpression of Shh at early stages, it is not known whether the reduced RGC growth seen *in vivo* is mediated by Shh acting directly as a guidance cue or, alternatively, as a morphogen causing re-patterning of the tissue and subsequent induction of guidance cues. Nonetheless, our model does not contradict these findings of *Shh* mRNA expression or the possibility that this Shh border has a role in establishing the location of the optic chiasm at early stages. However, we show that there is a predominant source of Shh protein at the chiasm itself that is not detected with *in situ* hybridization because it is retina derived. We demonstrate that the role of this retina-derived Shh at the chiasm is to selectively repel ipsilateral RGCs and that this repulsion is directly mediated by Shh signaling, as inhibition of *Smo* or inactivation of *Boc* in ipsilateral axons impairs their repulsive response to contralateral axons.

At the retina, *Shh* mRNA is expressed at E13.5 where it promotes and maintains the proliferation of retina precursor cells (Jensen and Wallace, 1997; Wang et al., 2005). Later, its expression is confined to RGC cell bodies, and this RGC-derived Shh promotes astrocyte proliferation along the optic nerve (Dakubo et al., 2008; Wallace and Raff, 1999). Intriguingly, in one study, researchers injected a radiolabel into the adult hamster retina, and they detected the accumulation of radiolabeled Shh in the superior colliculus, one of the final targets of RGCs (Traiffort et al., 2001). Thus, the authors speculated that this long-range transported Shh must have additional effects outside of the retina and optic nerve. Here we indeed find a guidance role for this Shh at a more anterograde site along the RGC axon—the optic chiasm—where protein secretion is the highest during development. We also detected Shh protein further along the axon in the optic tract, but additional roles for Shh at these more anterograde locations, including RGC target sites, remain to be elucidated.

The Repulsive Effect of Shh on Ipsilateral RGCs Is Localized to the Optic Chiasm

Our experiments with *in vitro* non-permeabilized Shh staining and *in vivo* Shh-pHluorin electroporations indicate that contralateral RGCs secrete Shh along the entirety of the axon. This raises the question of why repulsion of ipsilateral RGCs occurs only at

the optic chiasm. A first possibility is that ipsilateral RGCs are closely attuned to the levels of Shh protein, which we find is highest at the optic chiasm and lower at the optic nerve and tract. Furthermore, the selective upregulation of secretion at the optic chiasm, as shown by our Shh-pHluorin experiments, enhances the actual level of Shh encountered by ipsilateral RGCs. The mechanism for the enhanced secretion at the optic chiasm is currently unknown, but it may involve regulation of proteins that are involved in Shh processing and exocytosis such as Sortilin (Campbell et al., 2016) and other proteins such as Dispatched, Scube, and heparan sulfate proteoglycans (HSPGs), whose role in RGCs has not been examined (Creanga et al., 2012; Jakobs et al., 2016; Tukachinsky et al., 2012). In addition to axons preferentially secreting Shh at the chiasm, the convergence of the two optic nerves at the chiasm causes a doubling of the amount of Shh at the chiasm, potentially explaining the repulsion of ipsilateral axons at the chiasm. Thus, a repulsion concentration threshold may be reached at the optic chiasm, causing ipsilateral axons to turn away from the midline.

A second, non-exclusive possibility for chiasm-specific repulsion is that fasciculation dynamics along RGC axons affect the presentation of Shh to ipsilateral RGCs. In both the optic nerve and tract, ipsilateral axons grow fasciculated within their own bundle, which is segregated from contralateral axons (Jeffery and Erskine, 2005). It is unlikely that the lipid-modified, hydrophobic Shh (which is cholesterolated and palmitoylated) can penetrate significantly into the ipsilateral bundle and affect axons within this segregated bundle (Peters et al., 2004). Indeed, we find that, in *Boc* mutants, the segregation of the ipsilateral bundle is maintained in the optic nerve, consistent with the idea that Shh does not play a role in segregation within the optic nerve (Figure S4). In contrast, the optic chiasm is a site of major defasciculation of RGC axons, where extensive intermingling of ipsilateral and contralateral axons occurs (Baker and Jeffery, 1989). This context might allow ipsilateral RGCs to better detect the secreted Shh from neighboring contralateral axons, thus enabling a repulsive response. It will be interesting to see whether defasciculation at the optic chiasm is required for Shh-mediated repulsion of ipsilateral axons.

A third possibility is that other factors might modulate Shh activity and/or ipsilateral axon responsiveness to Shh. For example, a protein might increase the activity of Shh at the chiasm or, conversely, restrict its activity in the optic nerve. Alternatively, Shh responsiveness might be modulated at the level of *Boc* or its downstream effectors.

Intriguingly, this aspect of the precise spatiotemporal regulation of the axo-axonal response remains a mystery in many biological systems. For example, during specification of the olfactory bulb map topography, Semaphorin-3F (Sema3F) is secreted by olfactory neuron axons and deposited at the olfactory bulb to repel Neuropilin-2 (Nrp2)-positive axons that arrive later (Takeuchi et al., 2010). The sequential arrival of axons as well as the graded and complementary expression of Nrp2 and Sema3F by olfactory neurons helps to form the topographic order along the dorsoventral axis. While complementary expression of Nrp2 and Sema3F in olfactory neurons should, in theory, lead to repulsive axonal interactions before they reach the target, this is apparently not the case.

Interestingly, repulsion only occurs after the point of defasciculation of olfactory neuron axons and not before, similar to what we observe where repulsion follows defasciculation of RGCs at the optic chiasm.

Similarly, in the visual system, in addition to the ipsilateral–contralateral axon–axon midline segregation mechanism that we show here, Ephrin-A/EphA-mediated axon–axon interactions have been shown to play a role in the segregation of temporal and nasal axons at their target—the superior colliculus ([Suettelin and Drescher, 2014](#)). Again, despite Ephrin-A and EphA being expressed in the optic nerve and optic tract, we do not know what restricts the repulsive activity of Ephrin-A/EphA to the target. Undoubtedly, identifying these spatiotemporal regulation mechanisms will further our understanding of the complexity underlying the wiring of the nervous system.

An Additional Model for Choice Point Axon Guidance

Current understanding of axon guidance at midline choice points has generated a stereotypic model where cells at the midline produce a cue that attracts or repels axons from the midline. For example, in the developing spinal cord, floor plate cells secrete the chemoattractant Shh to guide commissural axons toward the midline ([Charron et al., 2003](#)), while Ephrin-B3 is expressed at the spinal cord midline to inhibit corticospinal tract neurons and interneurons in locomotor circuits from aberrantly crossing ([Kullander et al., 2001; Yokoyama et al., 2001](#)). At the optic chiasm, neighboring radial glial cells express Ephrin-B2, which repels ipsilateral RGCs, and also express VEGF164 and Sema6D to promote crossing of contralateral RGCs ([Erskine et al., 2011; Kuwajima et al., 2012; Williams et al., 2003](#)). Our study removes the conceptual constraint that midline guidance cues must be produced locally at the midline choice point by showing that

?

Shh at the optic chiasm is transported from the distant retina.

Intriguingly, it appears that the roles of midline glia-derived Ephrin-B2 and RGC-transported Shh are non-redundant, since the single inactivation of either *EphB1* or *Boc* leads to the loss of ipsilateral projections ([Fabre et al., 2010; Williams et al., 2003](#)). Thus, our study also demonstrates that locally produced cues can work together with remotely produced cues to play an important role in pathfinding at a midline choice point.

STAR★METHODS

Detailed methods are provided in the online version of this paper and include the following:

- KEY RESOURCES TABLE
- CONTACT FOR REAGENT AND RESOURCE SHARING
- EXPERIMENTAL MODEL AND SUBJECT DETAILS
 - Mice
- METHOD DETAILS
 - *In situ* hybridization and immunohistochemistry
 - Imaging and quantification
 - Constructs and siRNA reagents
 - *In utero* electroporation and enucleation of the retina
 - Optic chiasm whole-mount preparation
 - RGC explant culture and time-lapse imaging of axon interactions

- Time-lapse analysis
- Anterograde Dil tracing

● QUANTIFICATION AND STATISTICAL ANALYSIS

SUPPLEMENTAL INFORMATION

Supplemental Information includes four figures and two movies and can be found with this article online at <https://doi.org/10.1016/j.neuron.2017.12.028>.

ACKNOWLEDGMENTS

We thank Dr. Suzie Scales for providing us with the Shh antibody, Dr. Valerie Wallace for providing us with the ShhYFP construct, Dr. Marie Kmita for providing us with the Shh *in situ* probe plasmid, and Drs. Carol Mason and Stephen Brown for providing us with the Zic2 antibody. We thank Shirin Makihara and Lukas Tamayo-Orrego for help with blinding the drug treatments. We thank Dr. Patricia Yam for critical reading of the manuscript. This work was supported by grants from the Canadian Institutes of Health Research (CIHR) (334023), the Fonds de Recherche du Québec - Santé (FRQS) (27003), and the Canada Foundation for Innovation (CFI) (33768). J.P. was funded by a CIHR Vanier Canada Graduate Scholarship. F.C. holds the Canada Research Chair in Developmental Neurobiology.

AUTHOR CONTRIBUTIONS

Conceptualization, J.P., P.J.F., and F.C.; Methodology, J.P., P.J.F., T.D., T.S., and F.C.; Investigation, J.P., P.J.F., T.D., L.K., and S.M.S.; Writing – Original Draft, J.P.; Writing – Review & Editing, J.P. and F.C.; Funding Acquisition, F.C.; Supervision, F.C.

DECLARATION OF INTERESTS

The authors declare no competing interests.

Received: June 4, 2017

Revised: November 10, 2017

Accepted: December 15, 2017

Published: January 17, 2018

REFERENCES

- Ashby, M.C., Ibaraki, K., and Henley, J.M. (2004). It's green outside: tracking cell surface proteins with pH-sensitive GFP. *Trends Neurosci.* 27, 257–261.
- Badea, T.C., Cahill, H., Ecker, J., Hattar, S., and Nathans, J. (2009). Distinct roles of transcription factors brn3a and brn3b in controlling the development, morphology, and function of retinal ganglion cells. *Neuron* 61, 852–864.
- Baker, G.E., and Jeffery, G. (1989). Distribution of uncrossed axons along the course of the optic nerve and chiasm of rodents. *J. Comp. Neurol.* 289, 455–461.
- Beug, S.T., Parks, R.J., McBride, H.M., and Wallace, V.A. (2011). Processing-dependent trafficking of Sonic hedgehog to the regulated secretory pathway in neurons. *Mol. Cell. Neurosci.* 46, 583–596.
- Blacklaws, J., Deska-Gauthier, D., Jones, C.T., Petracca, Y.L., Liu, M., Zhang, H., Fawcett, J.P., Glover, J.C., Lanuza, G.M., and Zhang, Y. (2015). Sim1 is required for the migration and axonal projections of V3 interneurons in the developing mouse spinal cord. *Dev. Neurobiol.* 75, 1003–1017.
- Brown, L.Y., Kottmann, A.H., and Brown, S. (2003). Immunolocalization of Zic2 expression in the developing mouse forebrain. *Gene Expr. Patterns* 3, 361–367.
- Campbell, C., Beug, S., Nickerson, P.E., Peng, J., Mazerolle, C., Bassett, E.A., Ringuette, R., Jama, F.A., Morales, C., Christ, A., and Wallace, V.A. (2016). Sortilin regulates sorting and secretion of Sonic hedgehog. *J. Cell Sci.* 129, 3832–3844.
- Chan, S.O., Chung, K.Y., and Taylor, J.S. (1999). The effects of early prenatal monocular enucleation on the routing of uncrossed retinofugal axons and the

- cellular environment at the chiasm of mouse embryos. *Eur. J. Neurosci.* **11**, 3225–3235.
- Charron, F., Stein, E., Jeong, J., McMahon, A.P., and Tessier-Lavigne, M. (2003). The morphogen sonic hedgehog is an axonal chemoattractant that collaborates with netrin-1 in midline axon guidance. *Cell* **113**, 11–23.
- Chatzopoulou, E., Miguez, A., Savvaki, M., Levasseur, G., Muzerelle, A., Muriel, M.P., Gourreau, O., Watanabe, K., Goutebroze, L., Gaspar, P., et al. (2008). Structural requirement of TAG-1 for retinal ganglion cell axons and myelin in the mouse optic nerve. *J. Neurosci.* **28**, 7624–7636.
- Chung, K.Y., Leung, K.M., Lin, C.C., Tam, K.C., Hao, Y.L., Taylor, J.S., and Chan, S.O. (2004). Regionally specific expression of L1 and sialylated NCAM in the retinofugal pathway of mouse embryos. *J. Comp. Neurol.* **471**, 482–498.
- Creanga, A., Glenn, T.D., Mann, R.K., Saunders, A.M., Talbot, W.S., and Beachy, P.A. (2012). Scube/You activity mediates release of dually lipid-modified Hedgehog signal in soluble form. *Genes Dev.* **26**, 1312–1325.
- Dai, J., Buhusi, M., Demyanenko, G.P., Brennaman, L.H., Hruska, M., Dalva, M.B., and Maness, P.F. (2013). Neuron glia-related cell adhesion molecule (NrCAM) promotes topographic retinocollicular mapping. *PLoS ONE* **8**, e73000.
- Dakubo, G.D., Beug, S.T., Mazerolle, C.J., Thuring, S., Wang, Y., and Wallace, V.A. (2008). Control of glial precursor cell development in the mouse optic nerve by sonic hedgehog from retinal ganglion cells. *Brain Res.* **1228**, 27–42.
- Demyanenko, G.P., and Maness, P.F. (2003). The L1 cell adhesion molecule is essential for topographic mapping of retinal axons. *J. Neurosci.* **23**, 530–538.
- Dickson, B.J. (2002). Molecular mechanisms of axon guidance. *Science* **298**, 1959–1964.
- Echelard, Y., Epstein, D.J., St-Jacques, B., Shen, L., Mohler, J., McMahon, J.A., and McMahon, A.P. (1993). Sonic hedgehog, a member of a family of putative signaling molecules, is implicated in the regulation of CNS polarity. *Cell* **75**, 1417–1430.
- Erskine, L., Reijntjes, S., Pratt, T., Denti, L., Schwarz, Q., Vieira, J.M., Alakakone, B., Shewan, D., and Ruhrberg, C. (2011). VEGF signaling through neuropilin 1 guides commissural axon crossing at the optic chiasm. *Neuron* **70**, 951–965.
- Evans, T.A., and Bashaw, G.J. (2010). Axon guidance at the midline: of mice and flies. *Curr. Opin. Neurobiol.* **20**, 79–85.
- Fabre, P.J., Shimogori, T., and Charron, F. (2010). Segregation of ipsilateral retinal ganglion cell axons at the optic chiasm requires the Shh receptor Boc. *J. Neurosci.* **30**, 266–275.
- Flanagan, J.G., and Van Vector, D. (1998). Through the looking glass: axon guidance at the midline choice point. *Cell* **92**, 429–432.
- Garcia-Frigola, C., Carreres, M.I., Vegar, C., and Herrera, E. (2007). Gene delivery into mouse retinal ganglion cells by in utero electroporation. *BMC Dev. Biol.* **7**, 103.
- Godement, P., Salaün, J., and Métin, C. (1987). Fate of uncrossed retinal projections following early or late prenatal monocular enucleation in the mouse. *J. Comp. Neurol.* **255**, 97–109.
- Guillery, R.W. (1989). Early monocular enucleations in fetal ferrets produce a decrease of uncrossed and an increase of crossed retinofugal components: a possible model for the albino abnormality. *J. Anat.* **164**, 73–84.
- Harfe, B.D., Scherz, P.J., Nissim, S., Tian, H., McMahon, A.P., and Tabin, C.J. (2004). Evidence for an expansion-based temporal Shh gradient in specifying vertebrate digit identities. *Cell* **118**, 517–528.
- Herrera, E., Brown, L., Aruga, J., Rachel, R.A., Dolen, G., Mikoshiba, K., Brown, S., and Mason, C.A. (2003). Zic2 patterns binocular vision by specifying the uncrossed retinal projection. *Cell* **114**, 545–557.
- Jakobs, P., Schulz, P., Ortmann, C., Schürmann, S., Exner, S., Rebollido-Rios, R., Dreier, R., Seidler, D.G., and Grobe, K. (2016). Bridging the gap: heparan sulfate and Scube2 assemble Sonic hedgehog release complexes at the surface of producing cells. *Sci. Rep.* **6**, 26435.
- Jeffery, G. (2001). Architecture of the optic chiasm and the mechanisms that sculpt its development. *Physiol. Rev.* **81**, 1393–1414.
- Jeffery, G., and Erskine, L. (2005). Variations in the architecture and development of the vertebrate optic chiasm. *Prog. Retin. Eye Res.* **24**, 721–753.
- Jensen, A.M., and Wallace, V.A. (1997). Expression of Sonic hedgehog and its putative role as a precursor cell mitogen in the developing mouse retina. *Development* **124**, 363–371.
- Koch, S.M., Dela Cruz, C.G., Hnasko, T.S., Edwards, R.H., Huberman, A.D., and Ullian, E.M. (2011). Pathway-specific genetic attenuation of glutamate release alters select features of competition-based visual circuit refinement. *Neuron* **71**, 235–242.
- Kolpak, A., Zhang, J., and Bao, Z.Z. (2005). Sonic hedgehog has a dual effect on the growth of retinal ganglion axons depending on its concentration. *J. Neurosci.* **25**, 3432–3441.
- Kullander, K., Croll, S.D., Zimmer, M., Pan, L., McClain, J., Hughes, V., Zabski, S., DeChiara, T.M., Klein, R., Yancopoulos, G.D., and Gale, N.W. (2001). Ephrin-B3 is the midline barrier that prevents corticospinal tract axons from re-crossing, allowing for unilateral motor control. *Genes Dev.* **15**, 877–888.
- Kuwajima, T., Yoshida, Y., Takegahara, N., Petros, T.J., Kumanogoh, A., Jessell, T.M., Sakurai, T., and Mason, C. (2012). Optic chiasm presentation of Semaphorin6D in the context of Plexin-A1 and Nr-CAM promotes retinal axon midline crossing. *Neuron* **74**, 676–690.
- Lustig, M., Erskine, L., Mason, C.A., Grumet, M., and Sakurai, T. (2001). Nr-CAM expression in the developing mouse nervous system: ventral midline structures, specific fiber tracts, and neuropilar regions. *J. Comp. Neurol.* **434**, 13–28.
- Macdonald, R., Scholes, J., Strähle, U., Brennan, C., Holder, N., Brand, M., and Wilson, S.W. (1997). The Pax protein Noi is required for commissural axon pathway formation in the rostral forebrain. *Development* **124**, 2397–2408.
- Marcos, S., Nieto-Lopez, F., Sandonis, A., Cardozo, M.J., Di Marco, F., Esteve, P., and Bovolenta, P. (2015). Secreted frizzled related proteins modulate pathfinding and fasciculation of mouse retina ganglion cell axons by direct and indirect mechanisms. *J. Neurosci.* **35**, 4729–4740.
- Marcus, R.C., and Mason, C.A. (1995). The first retinal axon growth in the mouse optic chiasm: axon patterning and the cellular environment. *J. Neurosci.* **15**, 6389–6402.
- Miesenböck, G., De Angelis, D.A., and Rothman, J.E. (1998). Visualizing secretion and synaptic transmission with pH-sensitive green fluorescent proteins. *Nature* **394**, 192–195.
- Okada, A., Charron, F., Morin, S., Shin, D.S., Wong, K., Fabre, P.J., Tessier-Lavigne, M., and McConnell, S.K. (2006). Boc is a receptor for sonic hedgehog in the guidance of commissural axons. *Nature* **444**, 369–373.
- Peters, C., Wolf, A., Wagner, M., Kuhlmann, J., and Waldmann, H. (2004). The cholesterol membrane anchor of the Hedgehog protein confers stable membrane association to lipid-modified proteins. *Proc. Natl. Acad. Sci. USA* **101**, 8531–8536.
- Petros, T.J., Rebsam, A., and Mason, C.A. (2008). Retinal axon growth at the optic chiasm: to cross or not to cross. *Annu. Rev. Neurosci.* **31**, 295–315.
- Sánchez-Camacho, C., and Bovolenta, P. (2008). Autonomous and non-autonomous Shh signalling mediate the in vivo growth and guidance of mouse retinal ganglion cell axons. *Development* **135**, 3531–3541.
- Sankaranarayanan, S., De Angelis, D., Rothman, J.E., and Ryan, T.A. (2000). The use of pHluorins for optical measurements of presynaptic activity. *Biophys. J.* **79**, 2199–2208.
- Sloan, T.F., Qasaimeh, M.A., Juncker, D., Yam, P.T., and Charron, F. (2015). Integration of shallow gradients of Shh and Netrin-1 guides commissural axons. *PLoS Biol.* **13**, e1002119.
- Soares, C.A., and Mason, C.A. (2015). Transient ipsilateral retinal ganglion cell projections to the brain: Extent, targeting, and disappearance. *Dev. Neurobiol.* **75**, 1385–1401.
- Suettlerin, P., and Drescher, U. (2014). Target-independent ephrins/EphA-mediated axon-axon repulsion as a novel element in retinocollicular mapping. *Neuron* **84**, 740–752.

- Takeuchi, H., Inokuchi, K., Aoki, M., Suto, F., Tsuboi, A., Matsuda, I., Suzuki, M., Aiba, A., Serizawa, S., Yoshihara, Y., et al. (2010). Sequential arrival and graded secretion of Sema3F by olfactory neuron axons specify map topography at the bulb. *Cell* 141, 1056–1067.
- Tessier-Lavigne, M., and Goodman, C.S. (1996). The molecular biology of axon guidance. *Science* 274, 1123–1133.
- Tian, H., Callahan, C.A., DuPree, K.J., Darbonne, W.C., Ahn, C.P., Scales, S.J., and de Sauvage, F.J. (2009). Hedgehog signaling is restricted to the stromal compartment during pancreatic carcinogenesis. *Proc. Natl. Acad. Sci. USA* 106, 4254–4259.
- Torres, M., Gómez-Pardo, E., and Gruss, P. (1996). Pax2 contributes to inner ear patterning and optic nerve trajectory. *Development* 122, 3381–3391.
- Traiffort, E., Moya, K.L., Faure, H., Hässig, R., and Ruat, M. (2001). High expression and anterograde axonal transport of aminoterminal sonic hedgehog in the adult hamster brain. *Eur. J. Neurosci.* 14, 839–850.
- Trousse, F., Martí, E., Gruss, P., Torres, M., and Bovolenta, P. (2001). Control of retinal ganglion cell axon growth: a new role for Sonic hedgehog. *Development* 128, 3927–3936.
- Tukachinsky, H., Kuzmickas, R.P., Jao, C.Y., Liu, J., and Salic, A. (2012). Dispatched and scube mediate the efficient secretion of the cholesterol-modified hedgehog ligand. *Cell Rep.* 2, 308–320.
- Wallace, V.A., and Raff, M.C. (1999). A role for Sonic hedgehog in axon-to-astrocyte signalling in the rodent optic nerve. *Development* 126, 2901–2909.
- Wang, Y., Dakubo, G.D., Thurig, S., Mazerolle, C.J., and Wallace, V.A. (2005). Retinal ganglion cell-derived sonic hedgehog locally controls proliferation and the timing of RGC development in the embryonic mouse retina. *Development* 132, 5103–5113.
- Williams, S.E., Mann, F., Erskine, L., Sakurai, T., Wei, S., Rossi, D.J., Gale, N.W., Holt, C.E., Mason, C.A., and Henkemeyer, M. (2003). Ephrin-B2 and EphB1 mediate retinal axon divergence at the optic chiasm. *Neuron* 39, 919–935.
- Yokoyama, N., Romero, M.I., Cowan, C.A., Galvan, P., Heimbacher, F., Charnay, P., Parada, L.F., and Henkemeyer, M. (2001). Forward signaling mediated by ephrin-B3 prevents contralateral corticospinal axons from re-crossing the spinal cord midline. *Neuron* 29, 85–97.
- Zhang, X.M., and Yang, X.J. (2001). Regulation of retinal ganglion cell production by Sonic hedgehog. *Development* 128, 943–957.

STAR★METHODS**KEY RESOURCES TABLE**

REAGENT or RESOURCE	SOURCE	IDENTIFIER
Antibodies		
Anti-DIG-AP	Roche	Cat# 11 093 274 910; RRID:AB_2313640
Rabbit polyclonal anti-Shh	Gift of S. Scales (Genentech); (Tian et al., 2009)	RRID:AB_2716569
Rabbit polyclonal anti-Zic2	Gift of S. Brown (University of Vermont) via C. Mason (University of Columbia); (Brown et al., 2003 ; Herrera et al., 2003)	RRID:AB_2315623
Rabbit polyclonal anti-GFP	Thermo Fisher Scientific	Cat# A-11122; RRID:AB_221569
Rat monoclonal anti-mCherry	Thermo Fisher Scientific	Cat# M11217; RRID:AB_2536611
Mouse monoclonal IgM anti-Tag1	DSHB	Cat# 4D7/TAG1; RRID:AB_531775
Rabbit polyclonal anti-dsRed	Clontech Laboratories	Cat# 632496; RRID:AB_10013483
Mouse monoclonal anti-Neuron-specific beta-III Tubulin mAb (Clone TuJ-1)	R and D Systems	Cat# MAB1195; RRID:AB_357520
Chicken polyclonal anti-GFP	Abcam	Cat# ab13970; RRID:AB_300798
Goat polyclonal anti-Boc	Abcam	Cat# ab77556; RRID:AB_1565917
Rabbit polyclonal anti-Boc	This paper; (Fabre et al., 2010)	RRID:AB_2716570
Goat anti-rabbit IgG Alexa Fluor 488	Thermo Fisher Scientific	Cat# A-11034; RRID:AB_2576217
Goat anti-rat IgG Cy3	Jackson ImmunoResearch Labs	Cat# 112-165-143; RRID:AB_2338250
Goat anti-mouse IgM Alexa Fluor 488	Thermo Fisher Scientific	Cat# A-21042; RRID:AB_2535711
Goat anti-rabbit IgG Cy3	Jackson ImmunoResearch Labs	Cat# 111-165-144; RRID:AB_2338006
Goat anti-mouse IgG Alexa Fluor 488	Thermo Fisher Scientific	Cat# A-11029; RRID:AB_2534088
Donkey anti-goat IgG Alexa Fluor 488	Thermo Fisher Scientific	Cat# A-11055; RRID:AB_2534102
Donkey anti-rabbit IgG Cy3	Jackson ImmunoResearch Labs	Cat# 711-165-152; RRID:AB_2307443
Goat anti-mouse IgM Cy3	Jackson ImmunoResearch Labs	Cat# 115-165-075; RRID:AB_2338689
Goat anti-rabbit IgG Alexa Fluor 647	Jackson ImmunoResearch Labs	Cat# 711-605-152; RRID:AB_2492288
Chemicals, Peptides, and Recombinant Proteins		
DAPI	Sigma-Aldrich	Cat# D95964
Laminin	Thermo Fisher Scientific	Cat# 23017015
Laminin	Sigma-Aldrich	Cat# L2020
SANT-1	Calbiochem	Cat# 559303
Dil	Thermo Fisher Scientific	Cat# D282
Experimental Models: Organisms/Strains		
Mouse: C57BL/6	The Jackson Laboratory	RRID:IMSR_JAX:000664
Mouse: B6.Cg-Shh ^{tm1(EGFP/cre)Clt} /J	The Jackson Laboratory; (Harfe et al., 2004)	RRID:IMSR_JAX:005622
Mouse: B6.Cg-Gt(ROSA)26Sor ^{tm14(CAG-tdTomato)Hze} /J	Obtained from the colony of Y. Zhang (Dalhousie University); (Blacklaws et al., 2015)	RRID:IMSR_JAX:007914
Mouse: B6.FVB(Cg)-Tg(Slc6a4-cre/ERT2)EZ13Gsat/Mmucd	MMRRC; (Koch et al., 2011)	RRID:MMRRC_032109-UCD
Mouse: Boc ^{tm1Aok} /Boc ^{tm1Aok}	Obtained from the colony of A. Okada and S. K. McConnell (Stanford University); (Okada et al., 2006)	RRID:MGI:3696406

(Continued on next page)

Continued

REAGENT or RESOURCE	SOURCE	IDENTIFIER
Oligonucleotides		
siRNA targeting sequence: Shh #1: cacaagaaaactccgaacgatccaaggaa	This paper	N/A
siRNA targeting sequence: Shh #2: ctgttggaaaggcagggttcgactgggtct	This paper	N/A
Recombinant DNA		
RNA Probe: Shh (0.6kb)	Gift of M. Kmita (IRCM); (Echelard et al., 1993)	N/A
Plasmid: pCAGGS-ShhYFP	This paper; Subcloned from pCDNA3-ShhYFP, gift of V. Wallace; (Beug et al., 2011)	N/A
Plasmid: pCAGGS-Shh-pHluorin	This paper	N/A
Plasmid: pCAGGS-Shh (siRNA resistant)	This paper	N/A
Other		
μ-Slide 2 Well Ph+ Glass Bottom	Ibidi	Cat# 80297
Falcon 8 Well Culture Slide	BD Falcon	Cat# 354118

CONTACT FOR REAGENT AND RESOURCE SHARING

Further information and requests for reagents should be directed to and will be fulfilled by the Lead Contact, Frédéric Charron (frederic.charron@ircm.qc.ca). Shh antibody from Genentech was obtained through an MTA.

EXPERIMENTAL MODEL AND SUBJECT DETAILS**Mice**

All mice were maintained on a C57BL/6 genetic background (The Jackson Laboratory; RRID:IMSR_JAX:000664). The *Shh-Cre* line (B6.Cg-Shh^{tm1(EGFP/cre)Cjt/J}) was obtained from The Jackson Laboratory ([Harfe et al., 2004](#)). The *Slc6a4-Cre* line (B6.FVB(Cg)-Tg(Slc6a4-cre/ERT2)EZ13Gsat/Mmucl; RRID:MMRRC_032109-UCD) was obtained from MMRRC and previously described by [Koch et al. \(2011\)](#). The *tdTomato* line (B6.Cg-Gt(ROSA)26Sor^{tm1(CAG-tdTomato)Hze/J}; RRID:IMSR_JAX:007914) was kindly provided by Y. Zhang (Dalhousie University) ([Blacklaws et al., 2015](#)). The *Boc* line (*Boc*^{tm1Aok/Boc^{tm1Aok}; RRID:MGII:3696406) was kindly provided by A. Okada and S. K. McConnell (Stanford University) ([Okada et al., 2006](#)). Embryos of both (indeterminate) sexes were randomly chosen for immunostaining, electroporation, and explant studies at the ages and quantity specified in the figure legends. E0.5 was defined as noon on the date of plug discovery. All mice were housed in a specific pathogen-free barrier facility in static microinsulator cages, with up to 5 mice per cage at a temperature of 20–24°C and 40–70% humidity. Mice were maintained in a 12h light/dark cycle with autoclaved, UV treated water and a pelleted diet. All mice procedures were performed according to Canadian Council on Animal Care Guidelines and with approval from the Animal Care Committee at the Institut de Recherches Cliniques de Montréal.}

METHOD DETAILS***In situ* hybridization and immunohistochemistry**

In situ hybridization using DIG-labeled *Shh* RNA probe (plasmid kindly provided by M. Kmita) ([Echelard et al., 1993](#)) and immunohistochemistry were performed using standard protocols on embryonic heads fixed overnight in 4% PFA in PBS at 4°C (E10.5 spinal cords were fixed for 1 hour), washed 3 times with PBS, then transferred into 30% sucrose in PBS for 1–2 days before embedding in pure OCT and cryosectioning at 16 μm. Spinal cord sections underwent antigen retrieval with sodium citrate buffer for 1 hour at 95°C prior to blocking with 10% goat or donkey serum in PBS. Triton X-100 was added at 0.1% to the PBS used during and after the blocking step, except for non-permeabilized staining in which triton was never added. Primary antibodies were incubated at 4°C overnight and include (in order of use) Anti-DIG-AP (1:5000, Roche), rabbit anti-Shh (1:400, kindly provided by S. Scales, Genentech) ([Tian et al., 2009](#)), rabbit anti-Zic2 (1:10000, kindly provided by C. Mason and S. Brown, Columbia University) ([Brown et al., 2003](#)), rabbit anti-GFP (1:1000, Thermo Fisher), rat anti-mCherry (1:1000, Thermo Fisher), mouse anti-Tag1 (1:200, DSHB), rabbit anti-dsRed (1:1000, Clontech), mouse anti-Tuj1 (1:200, R&D Systems), chicken anti-GFP (1:1000, Abcam), goat anti-Boc (1:100, Abcam), rabbit anti-Boc (1:200, this paper and [Fabre et al., 2010](#)). Secondary antibodies conjugated with Alexa Fluor 488 (Thermo Fisher), Cy3 (Jackson ImmunoResearch), and Alexa Fluor 647 (Jackson ImmunoResearch) were used at 1:1000 and incubated for 1 h at room

temperature. DAPI (Sigma, 20mg/mL) was used at 1:10000 and incubated for 5 minutes at room temperature during the last wash before mounting in Mowiol (Sigma). Explants were stained directly in the 8-well culture slides (BD Falcon).

Imaging and quantification

Brightfield and Dil images were acquired on a Leica DM4000 microscope. Immunofluorescence images were acquired on Zeiss LSM700 and Leica SP8 confocal microscopes. Time-lapse imaging was performed on a Leica DMIRE2 inverted microscope with a heated chamber and a MS-2000 XYZ automated stage (ASI). 2x2 stitched phase-contrast images, centered on explants of interest, was captured every five minutes, with fluorescence images taken at the beginning and end of the time-lapse to identify ipsilateral axons.

Quantification of the intensity of immunofluorescent images was performed in ImageJ using the “mean gray value” to measure average intensity. The average intensity of the encircled area of interest was always background-corrected by subtracting the average intensity of an area of tissue adjacent to the area of interest. For heatmap images, the “16 Colors” lookup table of ImageJ was used.

Quantification of Dil images began with correction for uneven illumination by standardization of each image against a background fluorescent image taken of an orange-colored standardization slide, using a MATLAB macro. DAPI staining was used as a guide to encircle the optic tracts in Volocity 5.6, and the sum intensity values were recorded. This encircled region was then moved to an area of tissue adjacent to the optic tract to obtain the background sum intensity, which was subtracted to obtain the background-corrected optic tract value. The ipsilateral Dil percentage was calculated for each section as the intensity of ipsi/(contra+ipsi). The average of at least 3 sections of the optic tract was used to obtain the ipsilateral Dil percentage of each embryo.

Constructs and siRNA reagents

All electroporated constructs used were in the pCAGGS vector. The ShhYFP construct was a gift from Dr. Valerie Wallace and described previously (Beug et al., 2011). The Shh-pHluorin construct was made by subcloning superecliptic pHluorin into the same precursor construct used to make ShhYFP, thus occupying the exact position as YFP in the ShhYFP construct (immediately after Lys195). Shh siRNA experiments involved electroporation of a mix of 2 siRNA constructs at 5 μ M each, targeting nucleotides 200-227 and 496-523 of mouse Shh. A siRNA-resistant *Shh* construct was synthesized by GenScript using NM_009170.3 as the template with 6 silent point mutations introduced at the siRNA recognition sites (3 for each siRNA).

In utero electroporation and enucleation of the retina

In utero electroporation of the E13.5 retina was performed as previously described (Garcia-Frigola et al., 2007). Pregnant mice were injected with sustained-release buprenorphine intraperitoneally 6h prior to surgery. During surgery, mice were anesthetized with isoflurane, and a foot-pedal operated picospritzer (Parker) was used to inject approximately 1 μ L of the plasmid mixture containing 1 μ g/ μ L of each plasmid under the CAG promoter into the intraretinal space. Platinum plate electrode tweezers (Protech) connected to an ECM-830 electroporator (Harvard Apparatus) were placed across the eyes, with the positive electrode on the side with the electroporated eye, and 5 pulses of 35V were applied. To enucleate the eye, a fine-tip cauterizer was used (Fine Science Tools). The eye of the embryo was brought close to the uterine wall to minimize distance traveled by the cauterizer tip, and the tip brought into contact with the eye for 1 s, then withdrawn. The embryos were placed back and the opening was sutured and the skin clipped together.

Optic chiasm whole-mount preparation

The entire optic chiasm tissue, along with a portion of the optic nerve from electroporated E16.5 embryos was dissected in ice-cold PBS. The tissue was mounted in PBS between two glass #1.5 coverslips, with coverslip shards used as spacers. The preparation was immediately imaged with an inverted spinning disk confocal microscope (Zeiss Axio Observer with Yokogawa CSU-1). Then, the preparation was immersed in PBS containing 50 nM NH₄Cl to neutralize acidic intracellular vesicles, and the tissue was re-mounted and imaged again.

RGC explant culture and time-lapse imaging of axon interactions

RGC explants from E14.5-E16.5 wild-type or *Slc6a4-Cre* (*ipsi-Cre*); *tdTomato* retina were prepared as previously described (Fabre et al., 2010). Explants for time-lapse imaging were plated into 2-well glass-bottom chambers optimized for phase contrast imaging (Ibidi), while explants for immunohistochemistry were plated in 8-well culture slides (BD Falcon). Both chamber types received identical coating of PLL (Sigma) for two hours at room temperature, followed by 6 μ g/ μ L laminin (Sigma or Invitrogen) overnight at 37°C. For immunohistochemistry, the culture was fixed after 10-12 hours by adding 8% PFA to an equal volume of media for 20 minutes at room temperature, and explants were stained in the wells using immunohistochemistry protocols described above, prior to chamber disassembly and coverslip mounting in Mowiol (Sigma). For time-lapse experiments, imaging started 10-12 hours after explants were placed in the chambers at 37°C. In drug conditions, SANT-1 (135nM) or PBS was added to each of the chambers prior to imaging and the experimenter was blind to the treatment in each condition. Phase-contrast images were taken every 5 minutes in a 2x2 area centered around each explant of interest for 12 hours, while fluorescent images were taken only at the beginning and end of the time-lapse to identify ipsilateral RGC axons.

Time-lapse analysis

Time-lapse images were processed in ImageJ and viewed frame-by-frame to note for any instances where an extending growth cone (actor) encountered the axon or growth cone of another RGC (target). The identity of the actor and target RGCs (ipsi- or contralateral) was determined by following the RGCs to the beginning or end of the video, which contains the fluorescence image for identifying ipsilateral RGCs. The type of interaction was classified as “repulsion” only if the actor growth cone retracted or collapsed upon coming into direct or close ($< 20 \mu\text{m}$) contact with the target, and classified as “non-repulsion” in all other cases, including when the actor did not alter its trajectory and passed over the target, or when the actor fasciculated with the target axon. Although an actor may have multiple interactions with targets during the time-lapse, only the first interaction that each actor makes during the duration of the time-lapse was recorded. Actor growth cones that start out fasciculated with another axon when the time-lapse began were not analyzed.

Anterograde Dil tracing

Embryos that had been enucleated or electroporated at E13.5 were collected at E18.5 and the heads were collected into 12-well plates in 4% PFA in PBS overnight at 4°C. After 3 washes with PBS, each head was transferred to a PBS-filled Petri dish for dissection. The skin covering the eye was removed, a semicircular incision was made along the iris, and the lens removed. The head was transferred to a dry empty Petri dish, and the cornea flap was opened. The area inside and surrounding the eye was dried with a Kimwipe, but the retina was left moist with a small amount of PBS. Dil (Thermo Fisher) was placed into the retina with forceps and blended into a paste. Enough Dil was used to fill most of the cavity and the flap was closed. The heads were put back into PBS-filled 12-well plates, sealed with parafilm and covered with foil, and left on a low-speed shaker at 37°C for 14 days. The heads were then collected and embedded in OCT and cryosectioned coronally at 30 μm .

QUANTIFICATION AND STATISTICAL ANALYSIS

All statistical tests were performed using Prism 5 (GraphPad Software). All graphs were generated in Prism 5 except 100% contingency graphs in Figures 5C and 5D, which were generated with Microsoft Excel 2016. All error bars represent SEM and asterisks (*) indicate significance as follows: * $p < 0.05$, ** $p < 0.01$, *** $p < 0.001$, **** $p < 0.0001$, n.s. $p > 0.05$. The statistical analysis used in each experiment and the meaning of n are stated in the figure legends, and include paired two-tailed t test, two-tailed Student's t test, one-way repeated-measures ANOVA with Tukey's post test, two-way repeated-measures ANOVA with Bonferroni's post test, one-way ANOVA with Tukey's post test, and Fisher's exact test.

Supplemental Information

**Sonic Hedgehog Is a Remotely Produced
Cue that Controls Axon Guidance
Trans-axonally at a Midline Choice Point**

Jimmy Peng, Pierre J. Fabre, Tiphaine Dolique, Shannon M. Swikert, Laëtitia Kermasson, Tomomi Shimogori, and Frédéric Charron

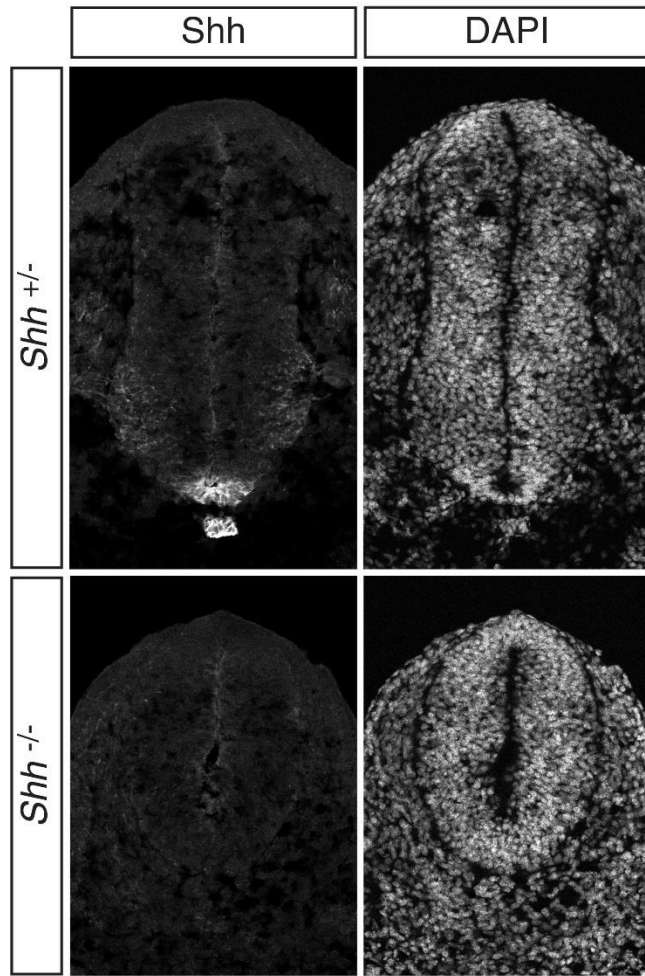


Figure S1. Related to Figure 1: Shh is detected specifically by the 95.9 rabbit anti-Shh polyclonal antibody. E10.5 mouse embryo sections were stained with the 95.9 Shh antibody, which detects Shh in the notochord and floor plate. This signal was lost when staining a *Shh*^{-/-} mutant.

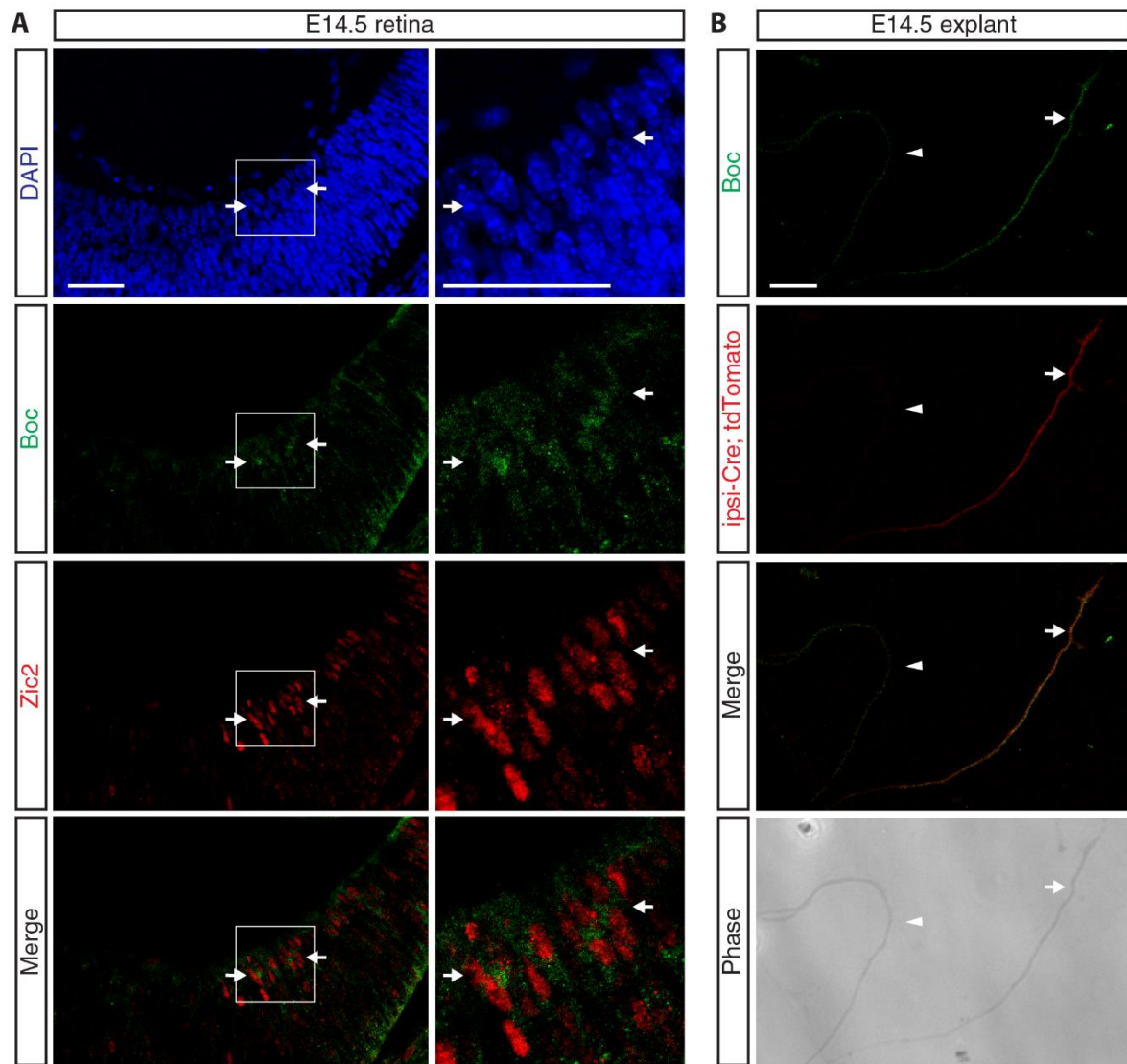


Figure S2. Related to Figure 3 and Figure 5: Boc is expressed by Zic2-positive cells and ipsi-Cre; tdTomato positive axons during midline crossing at E14.5. A) Immunofluorescence images of retina sections of wild-type E14.5 embryos stained with DAPI, Boc, and Zic2 antibodies. Areas of high expression of Boc, a membrane-bound receptor, can be detected surrounding RGC cell bodies positive for the Zic2 nuclear transcription factor (arrows). White boxes indicate the enlarged areas shown in the right column. B) Immunofluorescent and phase contrast images of RGC axons from an explant culture dissected from ipsi-Cre; tdTomato E14.5 embryos. The right RGC axon (arrow) is tdTomato-positive,

indicating it is an ipsilateral axon, and expresses Boc strongly. The left RGC axons (arrowhead) are tdTomato-negative and express residual levels of Boc. Scale bar = 20 μ m.

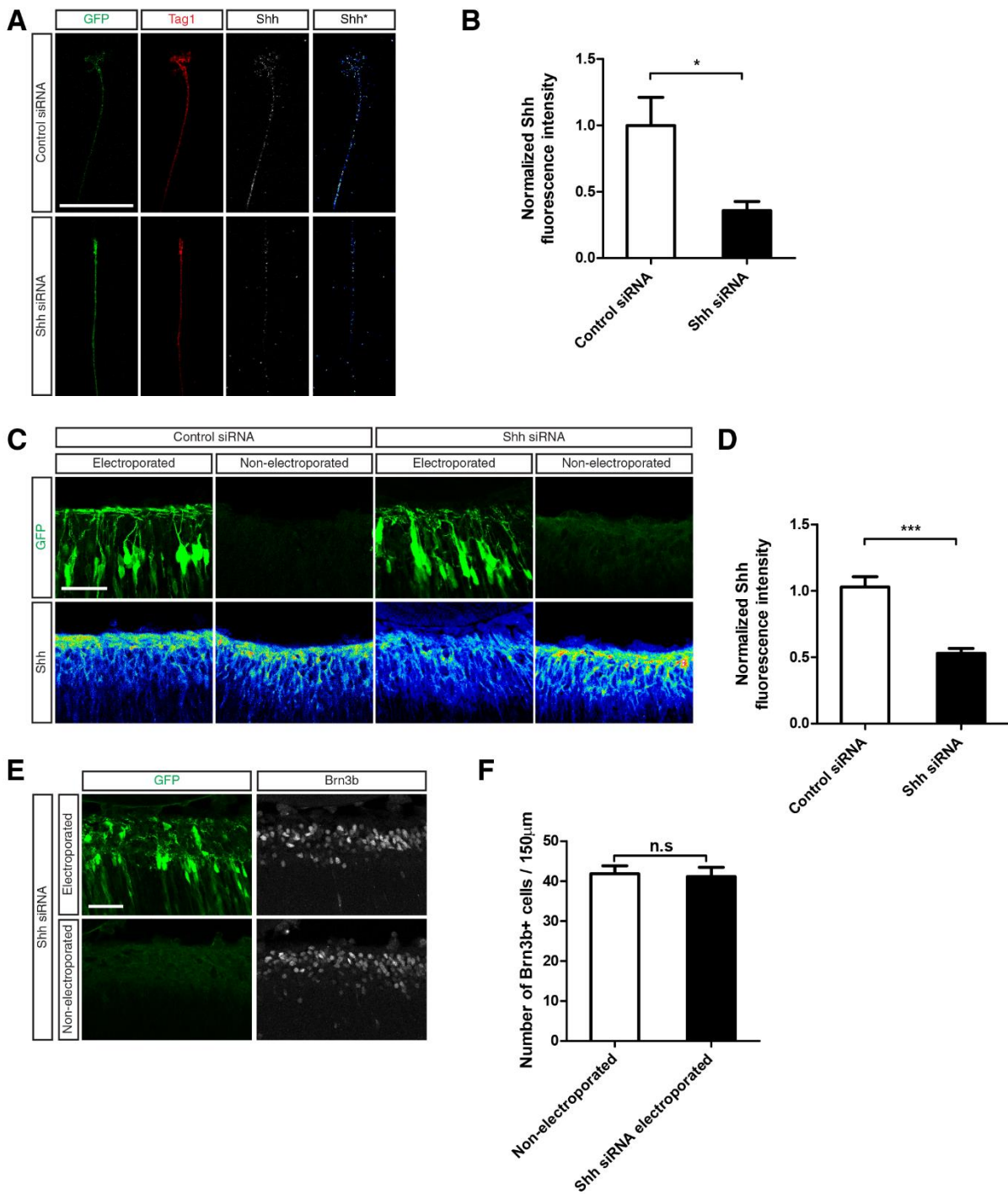


Figure S3. Related to Figure 6: *Shh* siRNA is effective at reducing endogenous *Shh* levels in RGCs and does not lead to perturbation in RGC specification when electroporated *in utero* at E13.5. A) Non-permeabilized immunofluorescent images of RGC axons from retina explants dissected from wild-type

E15.5 embryos, electroporated with control siRNA+GFP or *Shh* siRNA+GFP, labelled with the RGC marker Tag1 and Shh. Heatmap images of Shh intensity are shown in the *Shh** column. B) Quantification of the mean Shh fluorescence intensity of the axon and growth cones of RGCs electroporated with *Shh* siRNA and control siRNA, normalized to the average intensity for control siRNA. The mean Shh intensity is significantly lower in *Shh* siRNA electroporated RGCs compared to control siRNA (control: 1.0 ± 0.21 , *Shh*: 0.36 ± 0.07 , Student's two-tailed t-test, n=7 & 6, p=0.02). Data points from 7 control siRNA and 6 *Shh* siRNA-electroporated RGCs are included. C) Coronal sections of wild-type E15.5 retina co-electroporated with GFP along with control or *Shh* siRNA, immunostained with Shh antibody. Heatmap images of Shh intensity are shown in the lower panels. The Shh fluorescence intensity is reduced only in the portion of the retina electroporated with *Shh* siRNA. D) Quantification of the mean Shh fluorescence intensity in the RGC axon layer in GFP-positive areas of the retina electroporated with control versus *Shh* siRNA. Each mean Shh intensity value was normalized to an adjacent GFP-negative area of the same retina. The Shh fluorescence intensity was significantly reduced in the *Shh* siRNA electroporated retina compared to control siRNA (control: 1.03 ± 0.07 , *Shh*: 0.53 ± 0.04 , Student's two-tailed t-test, n=5 & 6, p=0.0002). Data points from 5 control siRNA retina and 6 *Shh* siRNA-electroporated retina are included, with each retina value being the average of at least 2 sections. E) Coronal sections of wild-type E17.5 retina co-electroporated with *Shh* siRNA and GFP, immunostained with the RGC transcription factor marker Brn3b. RGC cell numbers are unchanged in GFP-positive retina electroporated with *Shh* siRNA compared to non-electroporated retina. F) Quantification of Brn3b-positive cells in a 150 μm length of central retina in non-electroporated versus *Shh* siRNA-electroporated retina. The average number of Brn3b-positive cells is unchanged in non-electroporated versus *Shh* siRNA-electroporated retina (unelectroporated: 41.8 ± 2.0 , *Shh* siRNA electroporated: 41.1 ± 2.4 , Student's two-tailed t-test, n=4, p=0.83). Data points are from 4 single-eye *Shh* siRNA electroporated embryos. All error bars indicate SEM. n represents number of embryos. *p<0.05, ***p<0.001, n.s. p>0.05. Scale bar = 50 μm .

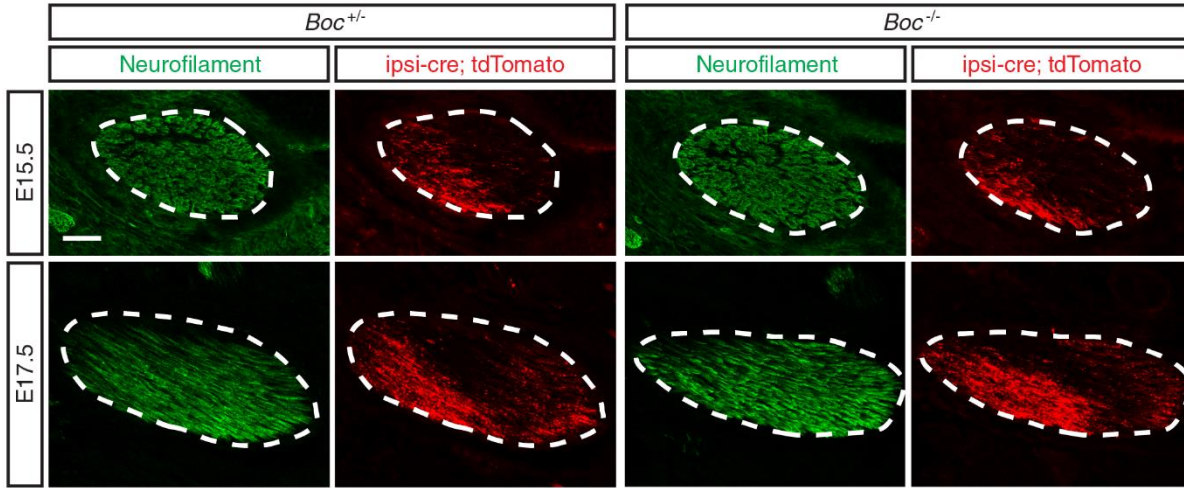


Figure S4. Related to Figure 6: *Boc* does not play a role in ipsilateral RGC segregation along the optic nerve. Coronal sections from E15.5 and E17.5 *ipsi-Cre; tdTomato* embryos were immunostained with the RGC marker neurofilament (NF-M) to visualize the optic nerve (white dashed outline) and anti-dsRed to visualize tdTomato-positive ipsilateral RGC axons. In both *Boc*^{+/-} and *Boc*^{-/-} animals, the ipsilateral RGC axons remain in the latero-ventral zone (bottom-left in all images) of the optic nerve. Scale bar = 50 μ m.